NJC

ROYAL SOCIETY OF CHEMISTRY

PAPER

View Article Online
View Journal | View Issue

Check for updates

Cite this: *New J. Chem.*, 2021, **45**, 7741

$NiFe_2O_4@SiO_2@ZrO_2/SO_4^{2-}/Cu/Co$ nanoparticles: a novel, efficient, magnetically recyclable and bimetallic catalyst for Pd-free Suzuki, Heck and C–N cross-coupling reactions in aqueous media†

Seyyedeh Ameneh Alavi G.,* Mohammad Ali Nasseri, Milad Kazemnejadi,
Ali Allahresani and Mahdi HussainZadeh

Received 22nd December 2020,
Accepted 30th March 2021

DOI: 10.1039/d0nj06208a

rsc.li/njc

The novel heterogeneous bimetallic nanoparticles of Cu–Co were synthesized based on magnetic nanoparticles, and the magnetic nanocatalyst was characterized by XRD, FE-SEM, EDX mapping, BET, TEM, HRTEM, FTIR, TGA, and VSM. This catalyst was successfully applied as a recyclable magnetically catalyst in Heck, Suzuki, and C–N cross-coupling reactions with various aryl halides (iodides, bromides, and chlorides as challengeable substrates), with olefins, phenylboronic acid, and amines, respectively. We considered the rise of synergetic effects from the different Lewis acid and Brønsted acid sites present in the catalyst. The catalyst was synthesized with cheap, available materials and a simple synthesis method. The catalyst can be separated easily using an external magnet. It was recycled for more than ten runs without a sensible loss of its catalytic activity, and no significant leaching of the Cu and Co quantity was observed. The significant benefits of the method are high-level generality, simple operation, and there are no heavy metals and toxic solvents. This is a quick, easy, efficacious and environmentally friendly protocol, and no by-products are formed in the reaction. These features make it an appropriate practical alternative protocol. In comparison with recent works, the other advantage of this catalyst is the synthesis of a wide variety of C–C and C–N bond derivatives (more than 40 derivatives). The other significant advantage is the low temperature of the reaction and the use of the least possible amount of the catalyst (0.003 g). The efficiency was good to excellent and the catalyst selectivity has been high. We aspire that our study inspires more interest to design novel catalysts based on using low-cost metal ions (such as cobalt and copper) in the cross-coupling reactions.

1. Introduction

The cross-coupling reaction is one of the basic reactions in the pharmaceutical industry and organic synthesis. The Heck and Suzuki reactions are the most convenient and efficient mechanisms to form C–C bonds.[1] These reactions are used to synthesize pharmaceutical, natural products, materials science, biological, medicinal, supramolecular chemistry, coordination chemistry, polymer synthesis, complex molecules, and are also used in catalysis.[2,3] Typically, Heck and Suzuki reactions are catalyzed by homogeneous catalysts, and this should be performed in high temperatures and toxic solvents.[4] The synthesis of efficient green catalysts has received more recent attention. These reactions are usually catalyzed by noble and transition metals, such as Ni,[5] Pd,[6] Ru,[7] Au–Pd,[8] Au–Ag–Pd,[9] and Pd–Ni.[10] The metals (such as palladium) are not recommended, because Pd cannot be industrialized exclusively due to its high cost and other important factors, such as scarce storage capacities. The toxicity and high cost of Pd catalysts restrict their applications.[11] Recent studies suggest that metal cobalt has a unique reactivity.[12,13] The metal cobalt changes its oxidation states and easily undertakes radical reactions.

Hence, it is not surprising that the cobalt metal is also widely involved in catalysis. There are many applications for metal cobalt, such as cross-couplings,[13] carbonylation reactions,[14] hydrogenations,[15] and functionalizations.[16]

Likewise, metal cobalt and copper catalysts have attracted the attention of researchers because of their applications. Copper catalysts have major advantages both economically and environmentally. They are available, cheap, and environment-friendly.[3]

In comparison with other transition metal catalytic systems, there have been numerous investigations for Cu and Co-catalyzed cross-coupling reactions, such as Heck and Suzuki. The latest

---

Department of Chemistry, Faculty of Science, University of Birjand, P. O. Box 97175-615, Birjand, Iran. E-mail: saalavi.g64@gmail.com

† Electronic supplementary information (ESI) available: ^{1}H-NMR and ^{13}C-NMR spectra of coupling products. See DOI: 10.1039/d0nj06208a

examples consist of Fe_3O_4@SiO_2@PrNCu,[17] MNP@PAMAM-Co,[12] Cu-NH_2-GO,[18] and Cu@MCOP[19] as catalysts for these reactions.

Bimetallic catalysis is an awesome way to perform chemical reactions that cannot be performed using single metal catalysis. The bimetallic catalyst procedure is different from single metal catalysts because both metals use special cycles that refer to transmetalation.[20] It is obvious that constructing a core–shell structure with another metal could change the electronic characteristics of the metal catalyst. This is mainly due to the relevance between the two separate metals. In addition to the relevance between metals, it provides more active sites for the catalysis mechanism in bimetallic nanoparticles.[21] Therefore, it has a great effect on the properties of the catalyst, especially on the performance of the catalyst. Consequently, bimetallic catalysts demonstrate a significant enhancement in catalytic activity in comparison with monometallic catalysts.[22] On the other hand, there is an incredible advantage for heterogeneous bimetallic catalysts, and it is tuning the catalytic activity. By controlling the dispersity, chemical composition, size, and shape of the metal nanoparticles, you can synthesize your choice based on the catalytic activity.[23]

Additionally, in this method, aryl chlorides were used as substrates. Aryl chlorides have advantages compared to bromides and iodides, such as availability, low cost, and they are more favourable and convenient in the Suzuki–Miyaura reactions.[24] Another incredible novelty is that these reactions led to the product with no palladium. The recent strategies are mainly related to the extensive use of organic solvents in organic transformations. One may expect that the organic solvents have undeniable destructive effects on human health and the environment. The cross-coupling reactions in aqueous environments is a difficult challenge that has attracted the attention of the synthetic community.[2] Thus, these reactions have restrictions, such as the catalytic system, mass transfer, and especially high temperature.[25] However, researchers are now trying to explore new low-temperature coupling strategies in aqueous systems.

One of the most applied solid acids with substantial catalytic activity is zirconium. It is used extensively as one of the best acid catalysts in many industries, such as petrochemical industries and oil refineries. This acid catalyst is used for processes like alkylation, cracking, esterification, and isomerization. Additionally, the activity of zirconium can be enhanced by sulfates.[26,27] Consequently, sulfated zirconium oxide (ZrO_2/SO_4^{2-}) can be produced with a great promotion in the catalytic activity. The sulfated zirconia has incredible features, such as outstanding catalytic activities, high thermal stability, high acidity, durability, and stability in various organic solvents. Under harsh reaction conditions, these characteristics rendered the sulfated zirconia as a suitable choice for more changes. It can also be industrialized and the catalytic aspects can be modified.[28] The catalytic activity has been examined in various organic reactions, for example, towards multicomponent reactions, benzylation reactions, and synthesis of α-aminophosphonates (Scheme 1).[29,30]

On the other hand, this fantastic sulfated zirconia can be magnetized by magnetic nanoparticles (MNPs). Magnetization *via* MNPs makes these supports magnetically recoverable. Another surprising thing is that due to the high aspect ratio, MNPs can strongly enhance the catalytic activity of a catalyst. In this article, $NiFe_2O_4$ NPs were used to support protocols. These NPs are popular and one of the most applicable nanomaterials, which consist of nickel and iron nanoparticles. They are widely used for various reactions due to their oxidation resistance, high thermal stability, high impregnation magnetization, low cost, flexibility in design, and low toxicity.[13] According to the previous result of our research team's publication, which consisted of the Sonogashira[3] coupling reaction, the synthesis of heterocyclic compounds (including xanthene[11] and quinolines[32]) from various starting materials and wide range of catalytic properties of the selected catalyst and its excellent performance in coupling reactions, we decided to extend the catalyst and investigate its application in other coupling reactions, such as Heck, Suzuki and also C–N coupling in a heterogeneous and bimetallic catalytic system due to the importance of using two metals in a system. The results have already been published, and the present study indicates the special properties of this catalyst and its extraordinary effectiveness in organic syntheses. In the present work, bimetallic nanoparticles were supported on magnetic $NiFe_2O_4$ NPs, and this catalyst was used for green Heck and Suzuki–Miyaura coupling reactions under moderate conditions. This bimetallic system awarded higher activity compared to its monometallic counterparts. Moreover, the effects of the Cu/Co ratio on the catalytic activity were investigated. After the recovery tests, it was shown that the catalyst did not significantly lose catalytic activity.

2. Experimental

2.1. Instrumentation and materials

All chemicals were bought from Merck, Sigma, and Fluka chemical companies. There was no need for further purification. The chemical solvents should be dried and distilled under a noble atmosphere before use. The progress of the reactions was monitored by thin-layer chromatography (TLC). The spectrum of FTIR was recorded by a JASCO FT/IR 4600 spectrophotometer with a KBr pellet. The NMR analyses (^1H and ^{13}C) were conducted by a Bruker Avance DPX-250 spectrometer, and $CDCl_3$ and DMSO-d_6 were used as a solvent. The TMS was an internal standard. The images of scanning electron microscopy (FE-SEM) were taken with a TESCAN MIRA3 apparatus. The mapping with transmission electron microscopy (TEM) was done with a Philips EM208 microscope, and the operation was conducted at 100 kV. The samples' magnetic behavior was determined at room temperature with Lake Shore Cryotronics 7407 (VSM). EDX spectra were recorded by a field emission scanning electron microscope (FE-SEM, JEOL 7600F), equipped with an energy dispersion of X-ray spectrometer from Oxford instruments. The samples (TGA) have been captured with a NETZSCH STA 409 PC/PG in N_2 atmosphere in the temperature range of 25–850 °C, and with a heating rate of 10 °C min^{-1}. The perusal of the magnetic properties of the samples was performed at room temperature by the Lake Shore Cryotronics 7407 vibrating sample magnetometer (VSM). Finally, ICP analysis was carried out

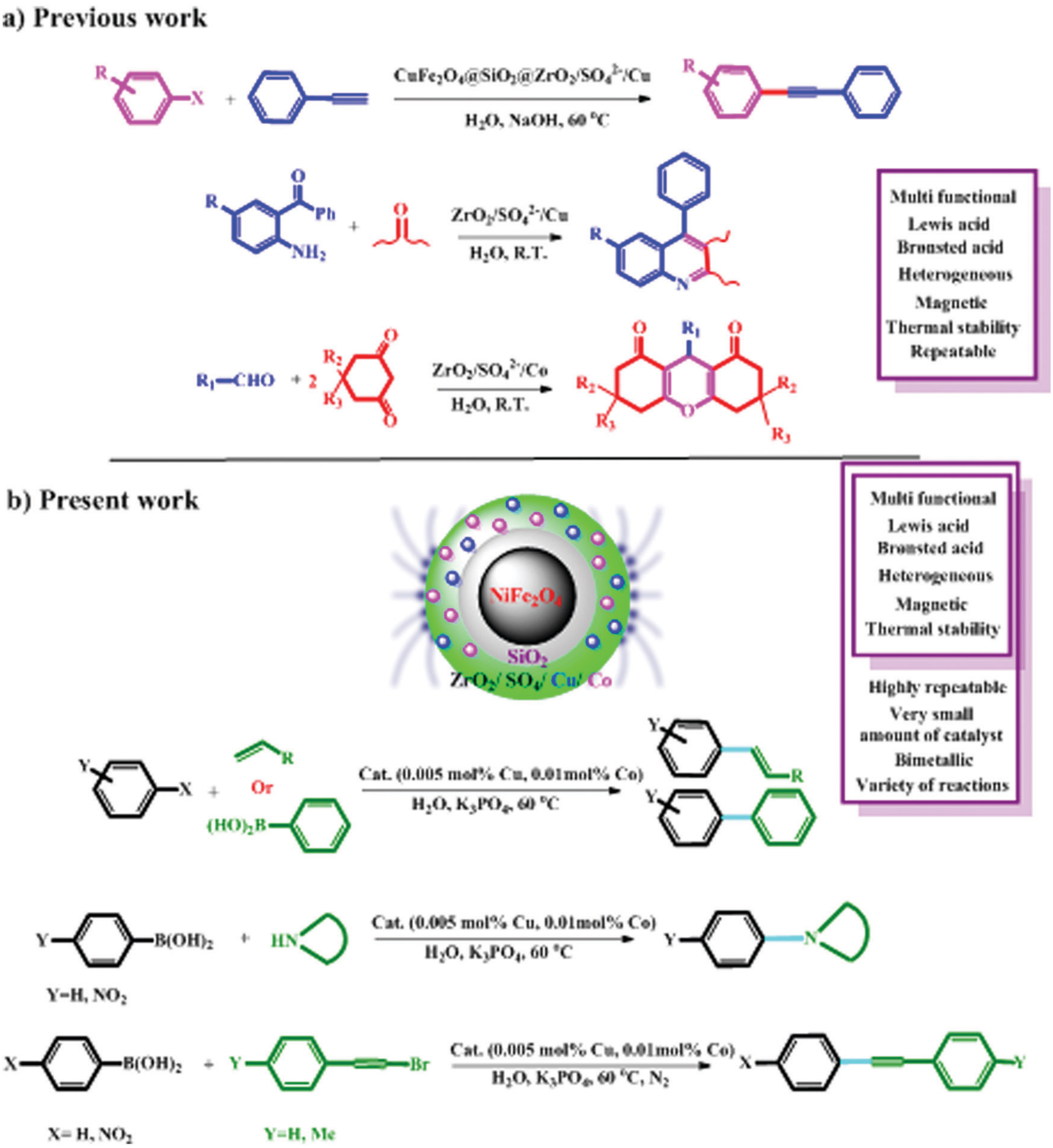

Scheme 1 The catalytic activity of metal incorporated into sulfated zirconium oxide for C–C and C–N cross-coupling reactions.

by VARIAN VISTA-PRO CCD simultaneous ICP-OES instrument. The surface area, pore diameter and pore volume of the nanoparticles were determined by Belsorp mini II instrument, and high resolution transmission electron microscopy (HRTEM) studies were performed on a FEI Tecnai G2 F20 Super Twin TEM with a field emission gun at 200 kV.

2.2. Preparation of $NiFe_2O_4@SiO_2$ MNPs

In a general process, 2.13 g $Fe(NO_3)_3 \cdot 9H_2O$ and 0.8 g $Ni(NO_3)_2 \cdot 6H_2O$ were dissolved in 150 mL DI water, and were stirred for at least 10 min. Eventually, the aqueous solution of NH_3 was added to the solution, and this process was ended at pH = 11. The obtained solution was stirred for 15 min, and then was treated at 180 °C for 12 h under static conditions by the hydrothermal method. The final product was washed several times with DI water and ethanol. At the end, it was dried at 60 °C in a vacuum oven.

$NiFe_2O_4@SiO_2$ MNPs were prepared by the sol–gel method. $NiFe_2O_4$ (2.0 g, 8.5 mmol) was dispersed in ethanol (25 mL) in an ultrasonic bath for 2 h at 60 °C. Then, the aqueous solution of ammonia (10 mL) was added to the mixture and was stirred at room temperature for at least 30 min. Subsequently, tetra ethoxy orthosilicate (TEOS, 1.0 mL) was added to the stirring mixture. The $NiFe_2O_4@SiO_2$ MNPs were separated from the solution by a magnetic field, washed with DI water (3 × 5 mL) and EtOH (2 × 5 mL), and then dried in a vacuum oven for at least 1 day. The final product $NiFe_2O_4@SiO_2$ MNPs were calcined at 400 °C for 4 h (at a heating rate of 20 °C min^{-1}).[31]

2.3. Preparation of $NiFe_2O_4@SiO_2@ZrO_2/SO_4^{2-}/Cu/Co$ NPs

The preparation proceeded according to the prepared sulfated zirconium oxide protocol that was previously reported, except with a modification.[3] First of all, $ZrCl_4$ (2.3 g, 10 mmol) was dissolved as a precursor in 10 mL water. Thus, an ammonia aqueous solution was added (10 mL, 1 N) drop by drop for 30 min until the pH was adjusted to 11. The provided suspended solution was aged for 24 h at room temperature. Then, the precipitation was washed with water using a centrifuge (5 × 10 mL). This process was ended after neutralization (pH = 7). The gained $Zr(OH)_4$ was dried at 100 °C for at least 1 day. The separated yield of $Zr(OH)_4$ was calculated to be 96% (1.5 g). Eventually, $Zr(OH)_4$ (1.0 g) was plunged with a mixing ratio of 1 : 3, Zr : S in $(NH_4)_2SO_4$ solution (2.5 g in 50 mL distilled water). The obtained solution was dried at 100 °C for 24 h. After drying, the precipitate was calcined at 650 °C for 3 h, and the rate of temperature was 10 °C min^{-1}. The resulting ZrO_2/SO_4^{2-} (1.0 g) was saturated by $Cu(OAc)_2$ solution (0.05 g in 50 mL distilled water) to obtain a Cu content of 5 wt%. This process was followed by drying at 100 °C for 12 h, and calcination at 400 °C for 3 h under air atmosphere (at a heating rate of 10 °C min^{-1}). The final obtained $ZrO_2/SO_4^{2-}/Cu$ was washed with water (3 × 10 mL), and then dried in an oven (50 °C) for 8 h.[32] The resultant $ZrO_2/SO_4^{2-}/CU$ (1.0 g) was impregnated in $Co(OAc)_2$ solution (0.05 g in 50 mL distilled water) in order to obtain a Co content of 5 wt%. The mixture was dried at 100 °C for 12 h, and subsequently calcinated at 400 °C for 3 h under air atmosphere (at a heating rate of 10 °C min^{-1}). The obtained $ZrO_2/SO_4^{2-}/Cu/Co$ was washed with water (3 × 10 mL), and then dried in the vacuum oven (50 °C) for 8 h.

The synthesized $ZrO_2/SO_4^{2-}/Cu/Co$ NPs were reinforced by $NiFe_2O_4@SiO_2$ magnetic nanoparticles. A mix of $NiFe_2O_4@SiO_2$ NPs (0.2 g) was dispersed in an ultrasonic bath in an aqueous solution of ethanol with a mixing ratio (15 mL, 1 : 3 v/v) for 10 min at room temperature. Another dispersed ethanolic solution of $ZrO_2/SO_4^{2-}/Cu/Co$ (0.4 g) was added to the mixture, and was dispersed for more than 10 min at room temperature. NaOH 10% w/w (15 mL) should be added drop by drop to the solution for 30 min during dispersion.

Finally, the solution was stirred for at least 1 day. The resulting $NiFe_2O_4@SiO_2@ZrO_2/SO_4^{2-}/Cu/Co$ NPs were separated by a magnetic field, washed with water, and was dried in a vacuum oven for 12 h. The full path to prepare the catalyst is shown in Scheme 2.

2.4. General procedure for the Suzuki–Miyaura and Heck–Mizoroki C–C coupling reactions using $NiFe_2O_4@SiO_2@ZrO_2/SO_4^{2-}/Cu/Co$ nanoparticles

A mixture of alkene/phenylboronic acid (1.5 mmol), aryl halide (1.0 mmol), $NiFe_2O_4@SiO_2@ZrO_2/SO_4^{2-}/Cu/Co$ magnetic nanocatalyst (0.003 g, (0.005 mol% Cu, 0.01 mol% Co)), K_3PO_4 (1.0 mmol) and water (1.0 mL) was stirred in an oil tub at 60 °C. The progress of the reaction was observed by TLC. According to the completion of the reaction, the mixture was extracted with 10 mL of ethyl acetate and the catalyst was removed magnetically. The merged organic layers were dried with Na_2SO_4. Then, under reduced pressure that was provided by rotary evaporator, the solvent was removed. The coupling pure favourable product was gained from the crude product by flash chromatography.

3. Results and discussion

3.1. Catalyst characterization

Different instruments conducted the characterization of synthesized catalyst. FTIR spectra of $Zr(OH)_4$, ZrO_2/SO_4^{2-}, $ZrO_2/SO_4^{2-}/Cu$, $ZrO_2/SO_4^{2-}/Co$, $ZrO_2/SO_4^{2-}/Cu/Co$, $NiFe_2O_4$, $NiFe_2O_4@SiO_2$, and $NiFe_2O_4@SiO_2@ZrO_2/SO_4^{2-}/Cu/Co$ are shown in Fig. 1. A wide and settled peak at 3403 cm^{-1} relating to the O–H stretch vibrations confirms the zirconium chloride hydration by using ammonia. Also, the 640–750 cm^{-1} absorptions relating to Zr–O–Zr can be seen at Fig. 1a. The FTIR spectra of ZrO_2/SO_4^{2-} illustrates the particular peaks at 1143, 1044, and 994 cm^{-1} (shoulder), which correspond to the symmetric and asymmetric stretch vibrations of S=O or S–O (Fig. 1b).[33] These vibrations introduce bidentate coordinated sulfate ions. Several peaks at 467–747 cm^{-1} are assigned to the Zr–O–Zr asymmetric stretch vibrations.[34] Also, a wide peak at 3421 cm^{-1} and a moderate peak at 1636 cm^{-1} were appointed to the O–H stretching and bending vibrations of the coordinated or adsorbed water with the sulfate groups, respectively. A sharp peak near 500 cm^{-1} was connected with the Cu–O stretching vibration. This illustrates that the

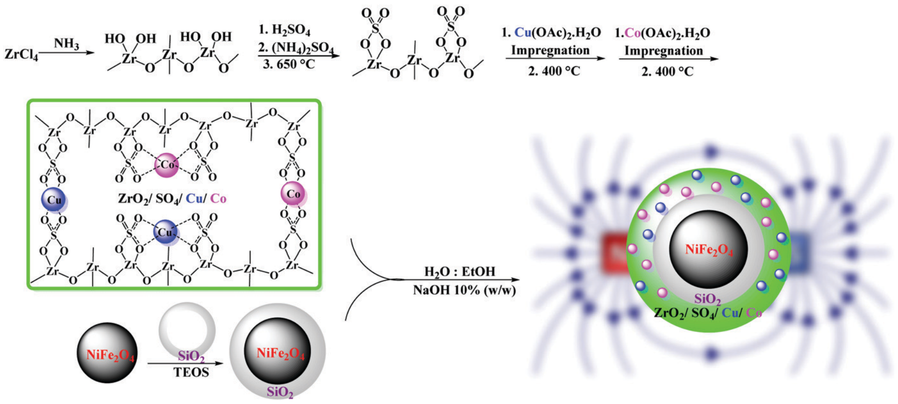

Scheme 2 Synthesis of the $NiFe_2O_4@SiO_2@ZrO_2/SO_4^{2-}/Cu/Co$ nanoparticles.

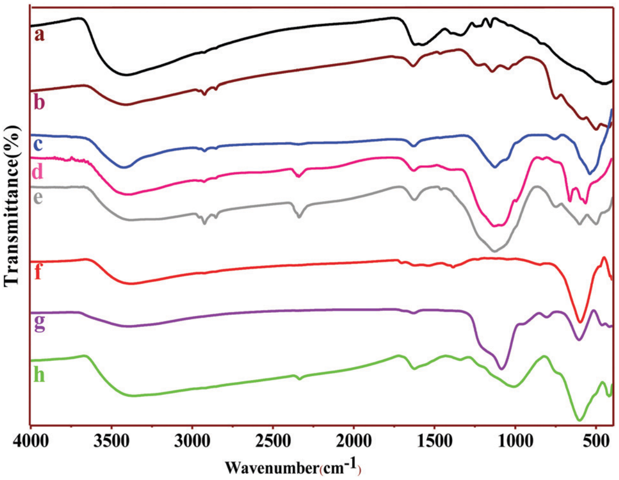

Fig. 1 FTIR spectra of (a) $Zr(OH)_4$, (b) ZrO_2/SO_4^{2}, (c) $ZrO_2/SO_4^{2-}/Cu$, (d) $ZrO_2/SO_4^{2-}/Co$, (e) $ZrO_2/SO_4^{2-}/Cu/Co$, (f) $NiFe_2O_4$, (g) $NiFe_2O_4@SiO_2$, (h) $NiFe_2O_4@SiO_2@ZrO_2/SO_4^{2-}/Cu/Co$.

compilation of Cu ions took place through the oxygen atoms of the sulfate ions in $ZrO_2/SO_4^{2-}/Cu$, and eventually accepted that the Cu cation was coordinated successfully in the catalyst framework (Fig. 1c).[32] The stretching vibrations relating to Zr–O–Zr are hidden because of strong absorption. A sharp peak at 566 cm^{-1} was put down to the Co–O stretching vibration, and it offers that the insertion of the Co ions took place through the oxygen atoms of the sulfate ions in $ZrO_2/SO_4^{2-}/Co$. This also affirms the successful coordination of the Co cations on the catalyst framework (Fig. 1d).[35]

In Fig. 1e, the presence of two strong peaks at 502 and 602 cm^{-1} indicates the coordination of both copper and cobalt metals. In the $NiFe_2O_4$ spectra of FTIR, two adsorption peaks at 1629 and 3374 cm^{-1} are attributed to the H–O–H bending and free O–H stretching vibrations, respectively. This is due to the water molecule adsorption on the surface of the $NiFe_2O_4$ NPs with a great aspect proportion.[36] There are two kinds of absorption bands at 476 and 596 cm^{-1} that were attributed to the Ni–O and Fe–O stretching vibrations (Fig. 1f).[36] A sharp absorption at 1084 cm^{-1} relating to the Si–O vibrations accepts the coating of $NiFe_2O_4$ NPs by silica shell (Fig. 1g).[31] The existence of vibrational bands near 481, 601, 1001 cm^{-1} showed Fe–O, (Cu–O and Co–O broad peak), and Si–O–Si respectively, and demonstrated that $ZrO_2/SO_4^{2-}/Cu/Co$ was supported on $NiFe_2O_4@SiO_2$ (Fig. 1h). Moreover, there were multiple medium bands in the 1261–1624 cm^{-1} region connected with the ZrO_2/SO_4^{2-} stretch vibrations (Fig. 1f).[3]

The XRD patterns of ZrO_2/SO_4^{2-}, $ZrO_2/SO_4^{2-}/Cu$, $ZrO_2/SO_4^{2-}/Cu/Co$, $NiFe_2O_4$, and $NiFe_2O_4@SiO_2@ZrO_2/SO_4^{2-}/Cu/Co$ are shown in Fig. 2. ZrO_2/SO_4^{2-} demonstrates three specific peaks with strong intensities at 2θ = 30.4°, 50.3°, and 60.2°, which indicates the tetragonal structure of ZrO_2/SO_4^{2-} with great crystallinity (JCPDS 17-0923) (Fig. 2a).[37] Indeed, a mixture of tetragonal and monoclinic phases can be seen in the spectra (Fig. 2a), which affirms the reported ZrO_2/SO_4^{2-} crystal structure.[38] The low intensity peaks at 2θ = 24.1° and 28.3° were attributed to

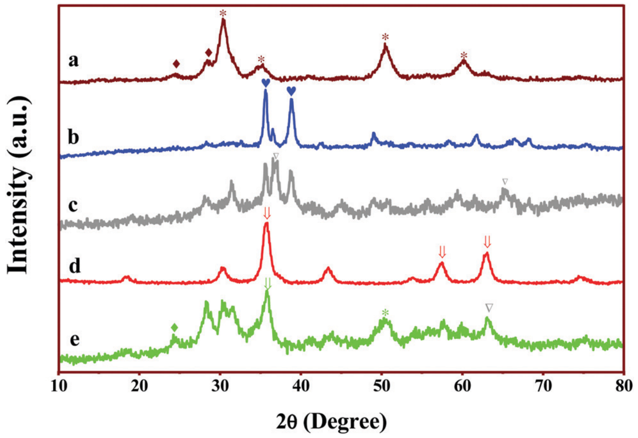

Fig. 2 XRD pattern of (a) ZrO_2/SO_4^{2}, (b) $ZrO_2/SO_4^{2-}/Cu$, (c) $ZrO_2/SO_4^{2-}/Cu/Co$, (d) $NiFe_2O_4$, (e) $NiFe_2O_4@SiO_2@ZrO_2/SO_4^{2-}/Cu/Co$.

the monoclinic structure of zirconia. It is a valuable notice that the existence of sulfated groups did not lead to the phase change of zirconia. This can be related to the strong interaction between the sulfate ions and zirconia. In addition, the presence of strong peaks in ZrO_2/SO_4^{2-} proves the trigonal structure, and it should be added that the saturation of the sulfate ions strongly affected the phase modification of zirconia from thermodynamically more stable monoclinic to the metastable tetragonal phase. Incorporation of Cu into the structure of ZrO_2/SO_4^{2-} causes a tiny shift in the position of the peaks relating to the crystal structure of sulfated zirconia at 2θ = 31.7°, 35.6°, 38.8°, 48.4°, 58.2°, 61.8°, 66.0° and 68.08°. Thus, the peaks at 2θ = 35.6°, 38.8°, 48.4°, 66.0°, and 68.08° have great matching with the indices (002), (111), (202), (311), and (113), respectively, which corresponds to the thermal prepared structure of the CuO powder (Fig. 2b).[28,29,32] Moreover, the sulfated zirconium oxide peaks were situated in the much lower intensities near the baseline (Fig. 2b). The addition of Co into the structure of ZrO_2/SO_4^{2-} leads to a new XRD pattern. These results suggest that the cobalt ions were successfully incorporated into the ZrO_2/SO_4^{2-} framework, and they took place through the sulfate ions according to the previous article.[35] In addition, new peaks appeared at

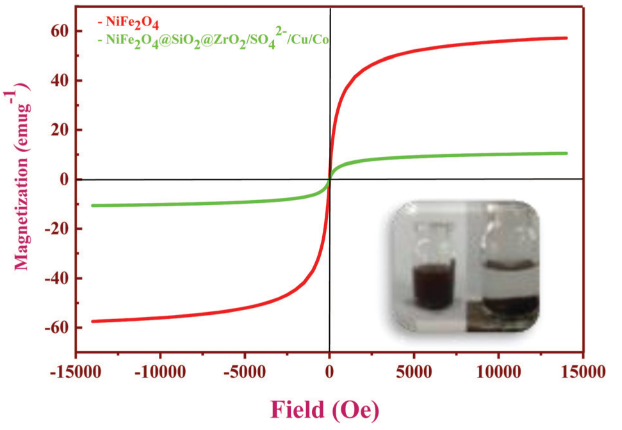

Fig. 3 Magnetic behavior of (a) $NiFe_2O_4$ and (b) $NiFe_2O_4@SiO_2@ZrO_2/SO_4^{2-}/Cu/Co$.

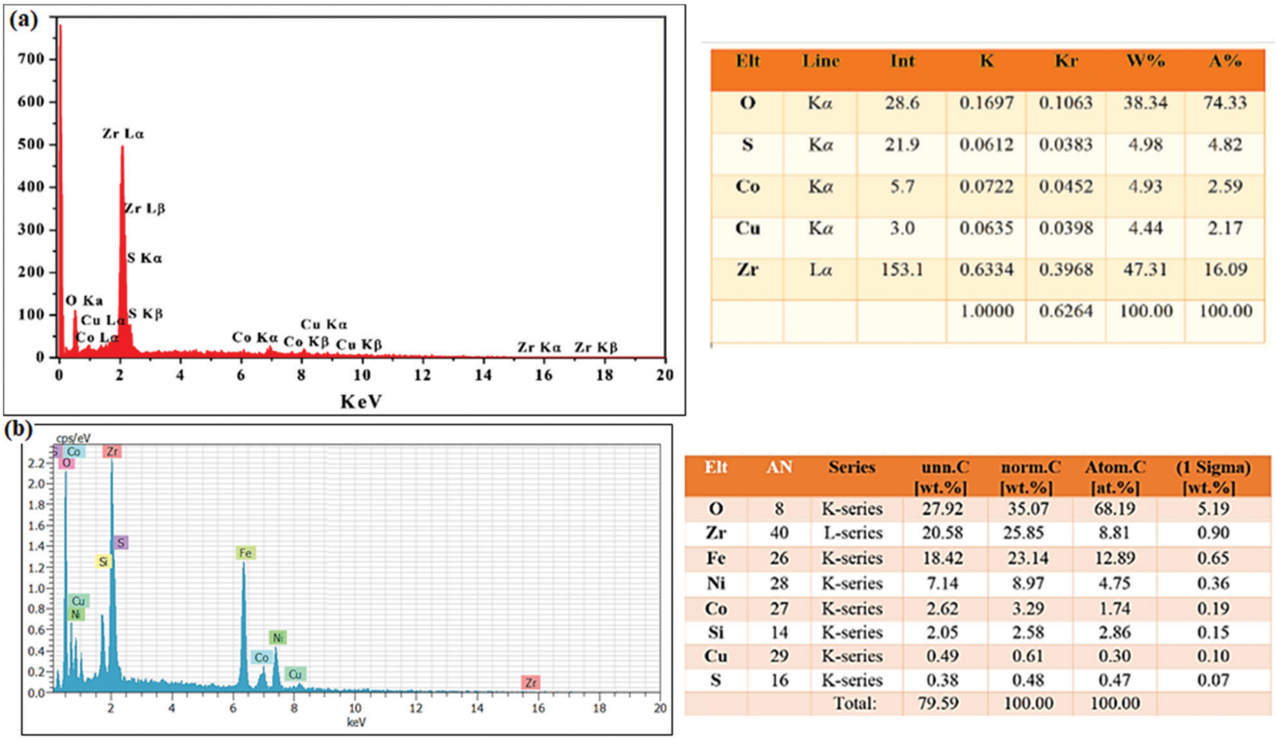

Elt	Line	Int	K	Kr	W%	A%
O	Kα	28.6	0.1697	0.1063	38.34	74.33
S	Kα	21.9	0.0612	0.0383	4.98	4.82
Co	Kα	5.7	0.0722	0.0452	4.93	2.59
Cu	Kα	3.0	0.0635	0.0398	4.44	2.17
Zr	Lα	153.1	0.6334	0.3968	47.31	16.09
			1.0000	0.6264	100.00	100.00

Elt	AN	Series	unn.C [wt.%]	norm.C [wt.%]	Atom.C [at.%]	(1 Sigma) [wt.%]
O	8	K-series	27.92	35.07	68.19	5.19
Zr	40	L-series	20.58	25.85	8.81	0.90
Fe	26	K-series	18.42	23.14	12.89	0.65
Ni	28	K-series	7.14	8.97	4.75	0.36
Co	27	K-series	2.62	3.29	1.74	0.19
Si	14	K-series	2.05	2.58	2.86	0.15
Cu	29	K-series	0.49	0.61	0.30	0.10
S	16	K-series	0.38	0.48	0.47	0.07
		Total:	79.59	100.00	100.00	

Fig. 4 EDX spectra of (a) $ZrO_2/SO_4^{2-}/Cu/Co$, (b) $NiFe_2O_4@SiO_2@ZrO_2/SO_4^{2-}/Cu/Co$.

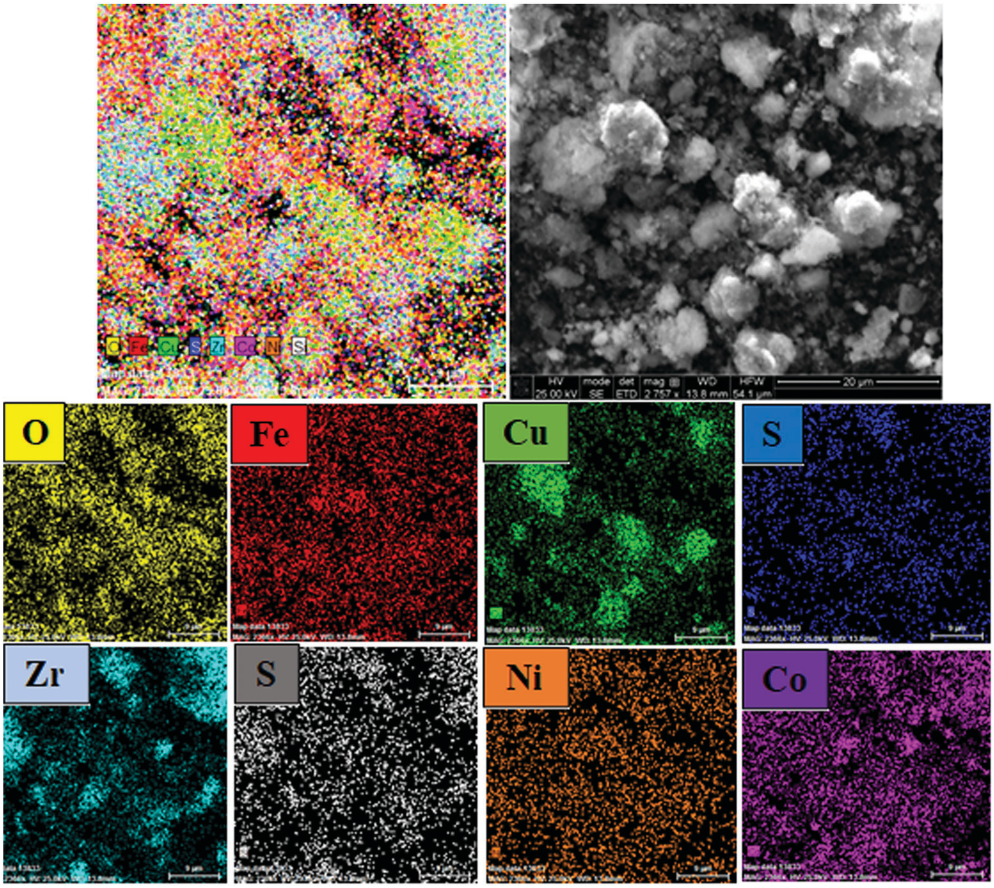

Fig. 5 TGA-DTG curves of (a) $ZrO_2/SO_4^{2-}/Cu/Co$, (b) $NiFe_2O_4@SiO_2@ZrO_2/SO_4^{2-}/Cu/Co$.

2θ = 38.3°, 43.6°, 62.09°, 75.5°, and 78.1°. These are in agreement with indices (111), (200), (220), (311), and (222), respectively, in accordance with the thermally prepared CoO powder structure. The addition of ionic metals into the ZrO_2/SO_4^{2-} matrix changes the XRD pattern of the matrix, and accepts the incorporation of the metal. The results show a proper dispersion of cobalt ions in the matrix of ZrO_2/SO_4^{2-}. The results offer a Co-O bond formation between the sulfate groups on ZrO_2/SO_4^{2-}/Co and Co ions.[35] The results demonstrate a Cu–O and Co–O bonding among the sulfated groups on ZrO_2/SO_4^{2-}/Cu/Co (Fig. 2c), and the Cu and Co ions are quite in accordance with its FTIR spectrum.

In the $NiFe_2O_4$ XRD pattern (Fig. 2d), the most severe peak was related to the (311) plane of the $NiFe_2O_4$ nanoparticles in 2θ = 35.62°.[39] Diffraction peaks were considered with 2θ values of 30.62°, 36.05°, 37.72°, 43.72°, 54.12°, 57.72°, 63.32°, which is compatible with the crystal planes (220), (311), (222), (400), (422), (511), (440) of the crystalline $NiFe_2O_4$, respectively, and the broad peak in the 10–30° region is related to $NiFe_2O_4$ covered by SiO_2.[40]

Fig. 2e shows the crystal structure of the catalyst, $NiFe_2O_4$@SiO_2@ZrO_2/SO_4^{2-}/Cu/Co supported by ZrO_2/SO_4^{2-} on the $NiFe_2O_4$@SiO_2 surface, resulting in the peaks with lower intensities related to the $NiFe_2O_4$ crystal structure. The results accept the functionalization of $NiFe_2O_4$ and did not lead to a changing phase. Furthermore, the sharp peak at 2θ = 38.2° illustrates the coordination of Cu and Co in the catalyst. The peaks at 2θ = 60.0°, 50.3°, 30.2°, and 50.7° might be appointed with the ZrO_2/SO_4^{2-} crystal structure. The $NiFe_2O_4$ functionalization with zirconium groups occurred successfully. The presence of

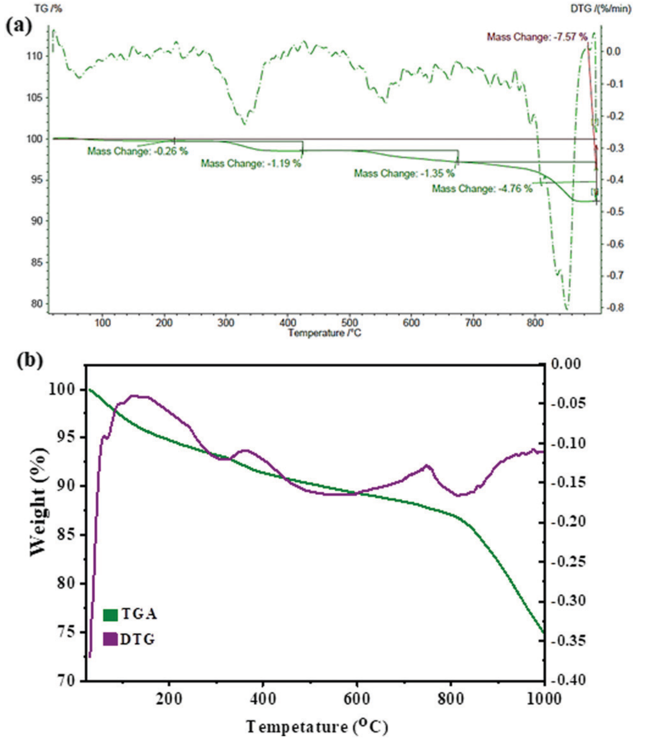

Fig. 6 TGA-DTG curves of (a) ZrO_2/SO_4^{2-}/Cu/Co, (b) $NiFe_2O_4$@SiO_2@ZrO_2/SO_4^{2-}/Cu/Co.

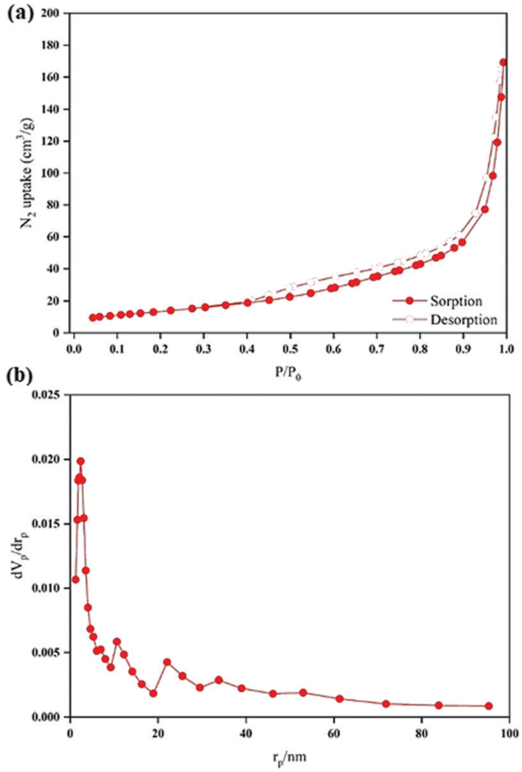

Fig. 7 (a) N_2 gas adsorption and desorption isotherms, and (b) the diameter distribution of the pores of $NiFe_2O_4$@SiO_2@ZrO_2/SO_4^{2-}/Cu/Co.

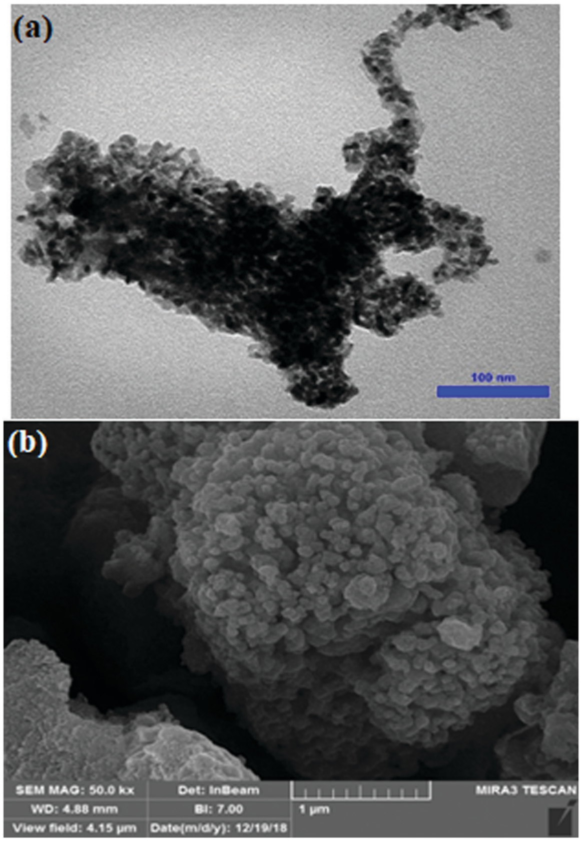

Fig. 8 (a) TEM and (b) FE-SEM images of ZrO_2/SO_4^{2-}/Cu/Co.

peaks related to the crystalline structure of $NiFe_2O_4$ confirms the change in the XRD pattern from the crystalline state to the amorphous state of $NiFe_2O_4@SiO_2@ZrO_2/SO_4^{2-}/Cu/Co$.

The magnetic properties of $NiFe_2O_4$ and $NiFe_2O_4@SiO_2@ZrO_2/SO_4^{2-}/Cu/Co$ were calculated by VSM analysis (Fig. 3). As shown in Fig. 3, these materials exhibited a superparamagnetic treatment, and no hysteresis loop was found in their spectra. The resultant $NiFe_2O_4$ saturation of magnetization was about 57.1 emu g^{-1} (Fig. 3a).[41]

The magnetization was largely reduced to 11.5 emu g^{-1} for $NiFe_2O_4@SiO_2@ZrO_2/SO_4^{2-}/Cu/Co$, which strongly affirms the surface functionalization (Fig. 3b). Thus, there is a sufficient magnetization for the complete separation of the nanoparticles from the mixture. The figures show the separation of $NiFe_2O_4@SiO_2@ZrO_2/SO_4^{2-}/Cu/Co$ from the mixture in 2 minutes with an external magnet after the dispersion.

The preparation of $ZrO_2/SO_4^{2-}/Cu/Co$ was accepted with the presence of Cu, Co, Zr, O, and S elements, and the detection was done by EDX analysis (Fig. 4a). Furthermore, the existence of the elements in the catalyst was checked and certified by EDX analysis. As shown in Fig. 4b, the presence of Zr, Cu, Co, O, S, Fe, Si, and Ni elements in the catalyst was confirmed.

In order to better identify the sample composition, elemental mapping analysis was performed. Fig. 5 shows the energy-dispersive X-ray spectroscopy (EDX) mapping analysis of Co, Cu, Ni, Si, S, Fe, Zr and O for the $NiFe_2O_4@SiO_2@ZrO_2/SO_4^{2-}/Cu/Co$ sample. The results ensure the presence of all of these elements in the sample, which are evenly distributed in the study section.

Accordingly, the successful association of Zr at the surface of $NiFe_2O_4@SiO_2$ was also confirmed by EDS map analysis.

The thermal treatment of $ZrO_2/SO_4^{2-}/Cu/Co$ and the catalyst can be seen in Fig. 6. The thermal stability of $ZrO_2/SO_4^{2-}/Cu/Co$ is considerable, and 7.5% weight loss at a temperature range of 25–1000 °C was observed (Fig. 6a). This degradation happened in a four-stage process. The first and second decreases could be appointed to the dehydration of the water adsorption from the surface of the catalyst (0.26% weight loss at 210 °C), and the evaporation of the trapped water in the network of the catalyst by sulfate groups (1.19% weight loss at 350 °C), respectively. The third weight loss was situated at the temperature range of 530–665 °C, and it is related to the oxidation of copper and cobalt, and the formation of CuO and Co–O. The final weight loss appeared at the temperature range of 680–860 °C. This is because of sulfate decomposition and the structural OH-groups. In the presence of $ZrO_2/SO_4^{2-}/Cu/Co$ on $NiFe_2O_4@SiO_2$, the thermal stability of the catalyst was maintained and 25.5% weight loss up to 1000 °C was observed. The first weight loss with a mild slope proceeded to 747 °C, and this is because of water adsorption in the catalyst crystal structure. The last weight loss was assigned to the

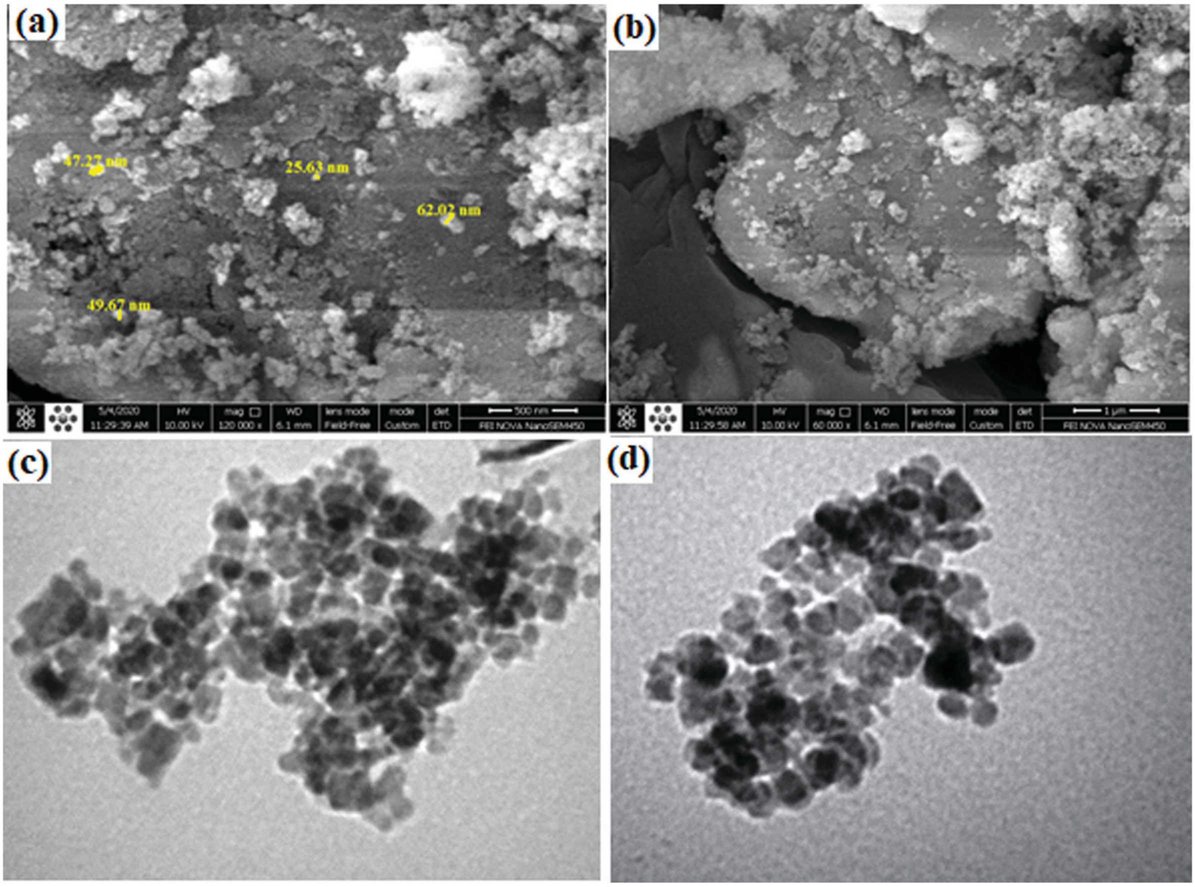

Fig. 9 (a) and (b) FE-SEM and (c) and (d) TEM images of $NiFe_2O_4@SiO_2@ZrO_2/SO_4^{2-}/Cu/Co$.

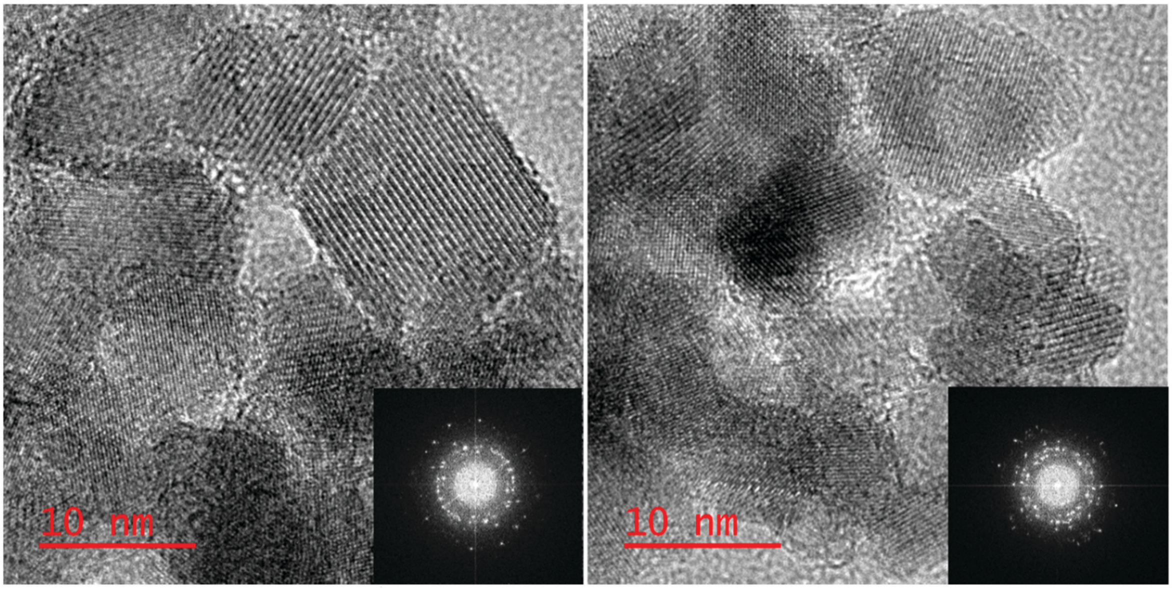

Fig. 10 HRTEM images of $NiFe_2O_4$@SiO_2@ZrO_2/SO_4^{2-}/Cu/Co.

decomposition of Cu and Co, and was incorporated with sulfate groups. This weight loss is around 19% (Fig. 6b).

The adsorption and desorption isotherms of nitrogen gas of the synthetic sample are shown in Fig. 7a. According to the IUPAC classification, the adsorption and desorption isotherms of nitrogen gas is type IV, which is the characterization of mesoporous materials. It also has an H3 hysteresis ring, which is the characteristic of plate-shaped porous materials. The specific surface area of the synthetic sample was measured using the BET method with an average surface area of 50.60 $m^2\ g^{-1}$. The size distribution of the sample cavities through the BJH desorption curve is shown in Fig. 7b. The highest pore volume is 0.24 $cm^3\ g^{-1}$, in which the pore diameter is 2.3 nm.[42,43]

The morphology and shape of ZrO_2/SO_4^{2-}/Cu/Co and $NiFe_2O_4$@SiO_2@ZrO_2/SO_4^{2-}/Cu/Co were extrapolated by SEM and TEM techniques (Fig. 8 and 9). The SEM images of ZrO_2/SO_4^{2-}/Cu/Co and $NiFe_2O_4$@SiO_2@ZrO_2/SO_4^{2-}/Cu/Co demonstrated an irregular amorphous morphology shape that arises from the expected accumulation in activated ZrO_2/SO_4^{2-} with transition metal inclusions (Fig. 8b and 9a, b). In comparison with their TEM images (Fig. 8a and 9c, d), this compression is more obviously shown. Based on Fig. 8b and 9a, b, the size of the particles has an average range of 12 nm and 42 nm for ZrO_2/SO_4^{2-}/Cu/Co and $NiFe_2O_4$@SiO_2@ZrO_2/SO_4^{2-}/Cu/Co, respectively.

HRTEM characterizations were measured to obtain a closer morphology and structure of the $NiFe_2O_4$@SiO_2@ZrO_2/SO_4^{2-}/Cu/Co composites. As shown in Fig. 10, the crystal planes of the different used metals in the catalyst rising from Cu and Co moieties incorporated in the ZrO_2/SO_4^{2-} framework have been distinguished by two different crystal structures. These two phases are clearly shown with two different crystal structures in Fig. 10. Also, the images were in agreement with the TEM and SEM images in terms of the average diameter, shape, and morphology.[44,45]

3.2. Optimization of the reaction parameters

In the coupling reaction of C–C, the determination of the optimized criteria was done by iodobenzene and styrene as a

Table 1 Optimization of the reaction parameters for the reaction of styrene and iodobenzene catalyzed by $NiFe_2O_4$@SiO_2@ZrO_2/SO_4^{2-}

Entry	Solvent	Base	Catalyst (g)	T. (°C)	*t*. (min)	Yield (%)	Entry	Solvent	Base	Catalyst (g)	T. (°C)	*t*. (min)	Yield (%)
1	EtOH	K_3PO_4	0.003	60	50	88	15	H_2O	NaOH	0.003	60	50	88
2	CH_3CN	K_3PO_4	0.003	60	50	62	16	H_2O	NaOAC	0.003	60	50	89
3	THF	K_3PO_4	0.003	60	50	48	17	H_2O	LiHMDS	0.003	60	50	60
4	CH_2Cl_2	K_3PO_4	0.003	60	50	62	18	H_2O	Et_3N	0.003	60	50	77
5	Toluene	K_3PO_4	0.003	60	50	77	19	H_2O	HMTA	0.003	60	50	58
6	$CHCl_3$	K_3PO_4	0.003	60	50	33	20	H_2O	*t*-BuOK	0.001	60	50	90
7	DMSO	K_3PO_4	0.003	60	50	90	21	H_2O	K_3PO_4	0.001	60	50	67
8	MeOH	K_3PO_4	0.003	60	50	89	22	H_2O	K_3PO_4	0.004	60	50	88
9	Dioxane	K_3PO_4	0.003	60	50	53	23	H_2O	K_3PO_4	0.006	60	50	94
10	DMF	K_3PO_4	0.003	60	50	70	24	H_2O	K_3PO_4	0.008	60	50	86
11	-	K_3PO_4	0.003	60	50	trace	25	H_2O	K_3PO_4	0.003	R.T.	50	70
12	**H_2O**	**K_3PO_4**	**0.003**	**60**	**50**	**93**	26	H_2O	K_3PO_4	0.003	80	50	96
13	H_2O	KOH	0.003	60	50	92	27	H_2O	K_3PO_4	0.003	Ref.	50	90
14	H_2O	K_2CO_3	0.003	60	50	67	28	H_2O	K_3PO_4	0.003	R.T.	240	78

Table 2 Mizoroki–Heck and Suzuki cross-coupling reaction catalyzed by the $NiFe_2O_4@SiO_2@ZrO_2/SO_4^{2-}$/Cu/Co NPs[a,b]

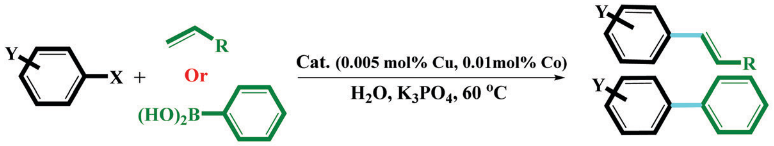

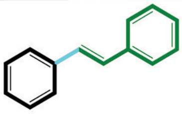

10a, X = I, 0.8 h, 93%,

10b, X = Br, 1 h, 92%,

10c, X = Cl, 3 h, 86%,

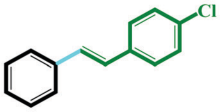

11a, X = I, 2 h, 81%,

11b, X = Br, 3.5 h, 78%

11c, X = Cl, 5 h, 73%

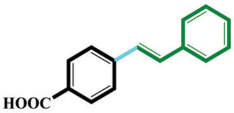

12a, X = I, 1 h, 91%

12b, X = Br, 1.5 h, 85%

12c, X = Cl, 3.5 h, 79%

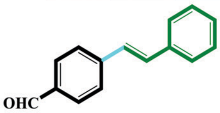

13a, X = I, 1.7 h, 80%

13b, X = Br, 2.4 h, 72%

13c, X = Cl, 3.8 h, 65%,

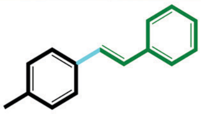

14a, X = I, 0.9 h, 92%

14b, X = Br, 1.3 h, 88%

14c, X = Cl, 3.4 h, 79%

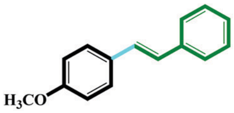

15a, X = I, 1.9 h, 77%

15b, X = Br, 3 h, 65%

15c, X = Cl, 5.5 h, 59%

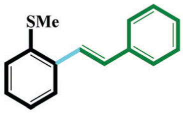

16a, X = I, 1.2 h, 89%

16b, X = Br, 1.8 h, 69%,

16c, X = Cl, 3.6 h, 55%

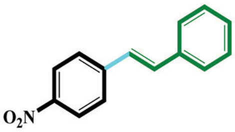

17a, X = I, 2 h, 56%

17b, X = Br, 3.8 h, 48%

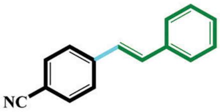

18a, X = I, 0.7 h, 89%

18b, X = Br, 1 h, 85%

18c, X = Cl, 3.5 h, 66%

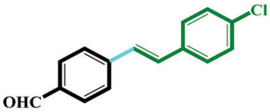

19a, X = I, 2.7 h, 59%

19b, X = Br, 5.9 h, 49%

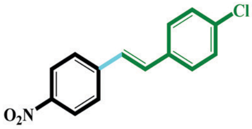

20a, X = I, 2.3 h, 66%

20b, X = Br, 5.8 h, 48%

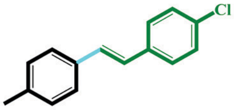

21a, X = I, 2.4 h, 68%

21b, X = Br, 6 h, 45%

21c, X = Cl, 8.8 h, 36%

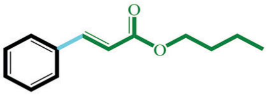

22a, X = I, 0.7 h, 92%

22b, X = Br, 1 h, 90%

22c, X = Cl, 3.1 h, 75%

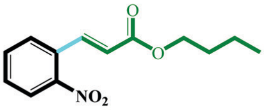

23a, X = I, 2 h, 76%

23b, X = Br, 4 h, 68%

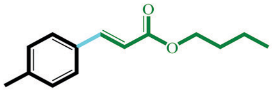

24a, X = I, 0.9 h, 89%

24b, X = Br, 1.5 h, 84%

24c, X = Cl, 3.8 h, 60%

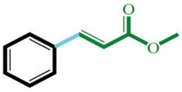

25a, X = I, 2 h, 90%

25b, X = Br, 3.2 h, 87%

25c, X = Cl, 7 h, 56%

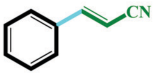

26a, X = I, 1.5 h, 78%

26b, X = Br, 2.5 h, 58%

26c, X = Cl, 4 h, 33%

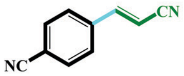

27a, X = I, 2 h, 66%

27b, X = Br, 2.5 h, 55%

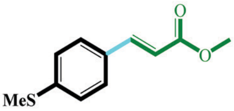

28a, X = I, 3 h, 70%

Table 2 (*continued*)

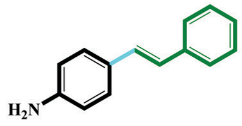

29a, X = I, 3 h, 61%
29b, X = Br, 6.5 h, 58%
29c, X = Cl, 10 h, 44%

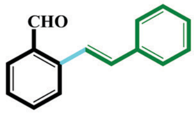

30a, X = I, 3 h, 67%

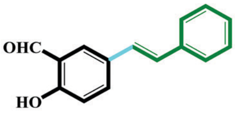

31a, X = I, 3 h, 78%
31b, X = Br, 5 h, 65%

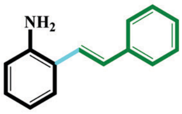

32a, X = I, 4 h, 58%
32b, X = Br, 8.5 h, 43%

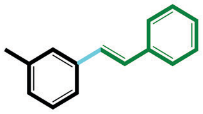

33a, X = I, 2 h, 80%
33b, X = Br, 3.5 h 72%
33c, X = Cl, 7 h, 59%

34a, X = I, 0.5 h, 94%
34b, X = Br, 1 h, 92%
34c, X = Cl, 1.8 h, 85%

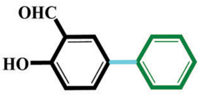

35a, X = I, 1.9 h, 82%
35b, X = Br, 2.3 h, 78%
35c, X = Cl, 5.4 h, 69%

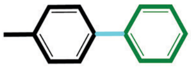

36a, X = I, 0.7 h, 92%
36b, X = Br, 1.3 h, 90%
36c, X = Cl, 2.5 h, 79%

37a, X = I, 1.5 h, 89%
37b, X = Br, 3 h, 78%
37c, X = Cl, 4.8 h, 55%

38a, X = I, 1.9 h, 81%
38b, X = Br, 3.3 h, 65%
38c, X = Cl, 6.8 h, 49%

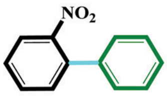

39a, X = I, 1.4 h, 82%
39b, X = Br, 3 h, 70%
39c, X = Cl, 5.5 h, 55%

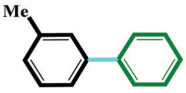

40a, X = I, 1 h, 86%
40b, X = Br, 3 h, 72%
40c, X = Cl, 4.8 h, 61%

41a, X = I, 1.2 h, 81%
41b, X = Br, 3.3 h, 68%
41c, X = Cl, 4 h, 57%

42a, X = I, 1.9 h, 73%
42b, X = Br, 3.9 h, 60%
42c, X = Cl, 5.5 h, 42%

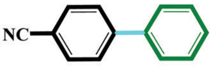

43a, X = I, 1 h, 80%
43b, X = Br, 2 h, 73%
43c, X = Cl, 3.8 h, 59%

44a, X = I, 1.7 h, 77%
44b, X = Br, 2.6 h, 68%
44c, X = Cl, 4.1 h, 54%

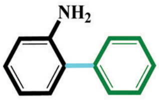

45a, X = I, 2.2 h, 68%
45b, X = Br, 3.8 h, 45%

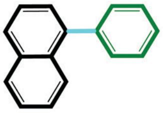

46a, X = I, 6.8 h, 61%
46b, X = Br, 7 h, 55%

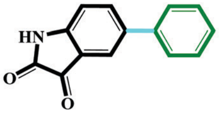

47a, X = I, 5.1 h, 53%

[a] The reaction conditions: Aryl halide (1.0 mmol), alkene/phenylboronic acid (1.5 mmol), K_3PO_4 (1.0 mmol), H_2O (1 mL), catalyst (0.003 g, (0.005 mol% Cu, 0.01 mol% Co)), 60 °C. [b] Isolated yields were reported.

model reaction. The effects of the reaction parameters, such as type of solvent, temperature, type of base, and catalyst amount, have investigated carefully. The results can be seen in Table 1. As shown in the results in polar protic solvents, such as EtOH,

Table 3 C–N cross-coupling reaction of phenylboronic acid with various amines catalyzed by the $NiFe_2O_4@SiO_2@ZrO_2/SO_4^{2-}/Cu/Co$ NPs[a,b]

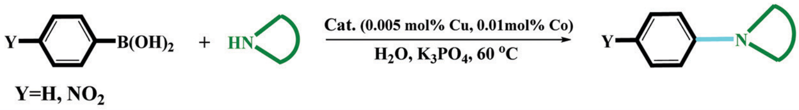

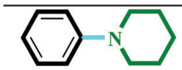

48a, Y=H, 2h, 87%

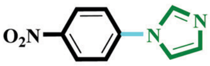

49a, Y=H, 1.6h, 91%

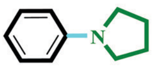

50a, Y=H, 1.9 h, 89%

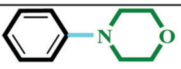

51a, Y=H, 2.4h, 70%

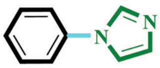

52a, Y=NO_2, 1.4h, 92%

[a] The reaction conditions: phenylboronic acid (1.0 mmol), *N*-heterocyclic compound (1.5 mmol), K_3PO_4 (1.0 mmol), H_2O (1 mL), catalyst (0.003 g, (0.005 mol% Cu, 0.01 mol% Co)), 60 °C. [b] Isolated yields were reported.

MeOH, and water (Table 1, inputs **1**, **8**, and **12**), the reaction was carried out at a constant time with a higher efficiency, which is in complete agreement with the structure of the catalyst containing the hydrophilic groups. The other solvents showed low to medium yields. Water was selected as the best solvent, and 90% efficiency was recorded in 50 minutes at 60 °C. Then, the effect of various bases was investigated over the model reaction in the presence of 0.003 g of $NiFe_2O_4@SiO_2@ZrO_2/SO_4^{2-}/Cu/Co$, and the effective temperature and varying amounts of the catalyst in optimal conditions were studied. The highest efficiency was obtained in 50 minutes in the presence of water solvent and base K_3PO_4 at 60 °C and 0.003 g of catalyst. (Table 1, entry 12).

The Heck carbon–carbon coupling reaction was investigated in the presence of various aryl halides, including electron donor and electron acceptor groups. After various studies and reaction optimization, in order to evaluate the range of reaction efficiency, its application in several different aryl halide derivatives was evaluated. The results presented in Table 2 show that the $NiFe_2O_4@SiO_2@ZrO_2/SO_4^{2-}/Cu/Co$ catalyst has an impressive efficiency in the synthesis of various diaryl derivatives.

The clear results show that the reaction efficiency of styrene with aryl iodides, including lethal electron groups such as NO_2, CN, and electron donor groups such as CH_3, and NH_2, are desirable (**14**, **16**, **18**, **29**). The reaction efficiency is comparable with the lethal electron group and the donor electron group aryl ions, and the efficiency was higher and the time was shorter for the lethal electron group aryl ions (comparison of compounds **16** and **29**, and others). The coupling reaction of the aryl iodides and aryl bromides was performed in a short time with appropriate efficiency, while the reaction of aryl chlorides in the longer reaction time produces a product with desired efficiency, which can be due to less reactivity, the C–Cl bond and the difference in the halogen cracking ability (I > Br > Cl) (comparison of compounds **18a** and **18c**, and others).

Table 4 C–C cross-coupling reaction of phenylboronic acid with (bromoethynyl)benzene catalyzed by the $NiFe_2O_4@SiO_2@ZrO_2/SO_4^{2-}/Cu/Co$ NPs[a,b]

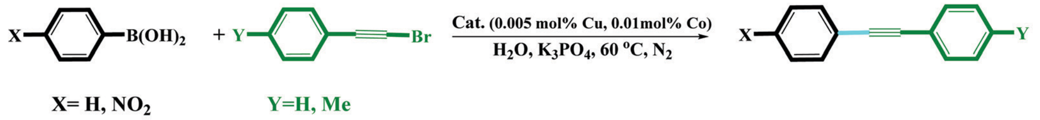

53a, 1h, 87%

54a, 1.3h, 81%

55a, 0.9 h, 89%

[a] The reaction conditions: phenylboronic acid (1.0 mmol), (bromoethynyl)benzene (1.5 mmol), K_3PO_4 (1.0 mmol), H_2O (1 mL), catalyst (0.003 g, (0.005 mol% Cu, 0.01 mol% Co)), 60 °C. [b] Isolated yields were reported.

Table 5 Control experiments for the reaction of styrene and phenylboronic acid with iodobenzene catalyzed by $NiFe_2O_4@SiO_2/ZrO_2/SO_4^{2-}/Cu/Co$

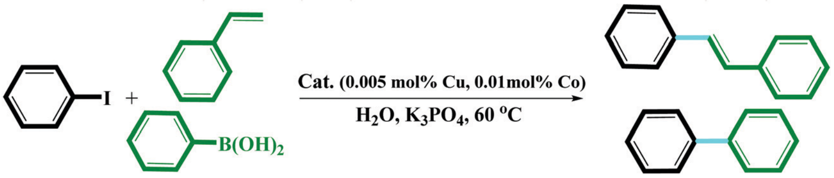

Entry	Cat. (0.003 g)	Time (h)	Yield (%)	
			10a[a]	**34a**[b]
1	No Catalyst	24	No reaction	No reaction
2	$ZrCl_4$	24	No reaction	No reaction
3	$(NH_4)_2SO_4$	24	No reaction	No reaction
4	ZrO_2/SO_4^{2-}	24	No reaction	No reaction
5	$Cu(OAC)_2$	24	No reaction	No reaction
6	$Co(OAC)_2$	24	No reaction	No reaction
7	$NiFe_2O_4$	24	21	26
8	$NiFe_2O_4@SiO_2$	24	15	19
9	$NiFe_2O_4@SiO_2/SO_4^{2-}/Cu/Co$	1	53	55
10	$ZrO_2/SO_4^{2-}/Cu$	1	71	78
11	$ZrO_2/SO_4^{2-}/Co$	1	68	72
12	$ZrO_2/SO_4^{2-}/Cu/Co$	1	81	83
13	$\mathbf{NiFe_2O_4@SiO_2/ZrO_2/SO_4^{2-}/Cu/Co}$	**0.8**	**93**	**94**

[a] Reaction conditions: iodobenzene (1.0 mmol), styrene (1.5 mmol), Cat. (0.003 g), H_2O (1 mL), 60 °C. [b] Reaction conditions: iodobenzene (1.0 mmol), phenylboronic acid (1.5 mmol), Cat. (0.003 g), H_2O (1 mL), 60 °C.

In order to expand the work and evaluate the high efficiency of the $NiFe_2O_4@SiO_2@ZrO_2/SO_4^{2-}/Cu/Co$ catalyst, the carbon–carbon coupling reaction with various substrates, including butyl acrylate and methyl acrylate, was investigated. The results are shown in Table 2, which showed excellent results.

Due to the excellent results obtained from the Heck coupling reaction and the high performance of the $NiFe_2O_4@SiO_2@ZrO_2/SO_4^{2-}/Cu/Co$ catalyst, the optimal conditions obtained for the Heck reaction, the Suzuki coupling reaction, and the carbon-nitrogen coupling were also investigated. The results are shown in Tables 2 and 3. A specific type of carbon–carbon coupling was obtained by reacting (bromoethynyl)benzene with boronic acid under optimal conditions (Section 3-2) and in the presence of nitrogen gas, which leads to the synthesis of 1,2-diphenylethyne compounds to the range of activities that the $NiFe_2O_4@SiO_2@ZrO_2/SO_4^{2-}/Cu/Co$ catalyst was also added (compounds **53**, **54**, and **55** (Table 4)).

3.3. Control experimental

In order to reassure the performance of the specific catalytic activity of the catalyst, the reaction was carried out in the absence of catalysts and the individual components of the catalyst for the synthesis of 1,2-diphenylethene (**10a**) (Table 5). The results showed that all parts of the catalyst could work together effectively (synergistic effect). In the absence of a catalyst and in the presence of compounds $ZrCl_4$, $(NH_4)_2SO_4$, ZrO_2/SO_4^{2-}, $Cu(OAC)_2$, $Co(OAC)_2$, no product was observed over 24 hours. The $NiFe_2O_4$ and $NiFe_2O_4@SiO_2$ efficiencies were about 21% and 15%, respectively. By coordinating copper or cobalt $ZrO_2/SO_4^{2-}/Cu$, $ZrO_2/SO_4^{2-}/Co$, the efficiency was increased to 71% and 68%, respectively. In the bimetallic system, the efficiency was increased to 81%, which represents an increase in the catalytic activity. In entry 9, it can be seen that despite all the parts of the catalyst except zirconium, high efficiency has not been achieved, which shows the significant effect of zirconium. Finally, by connecting

Table 6 Comparison of the catalytic activity of $NiFe_2O_4@SiO_2@ZrO_2/SO_4^{2-}/Cu/Co$ NPs with literature examples for **10b**, **36c**, **22a**, **50a**, **25b**

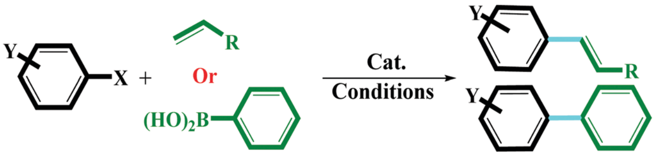

Run		Catalyst	Condition	Time (h)	Yield (%)	Ref.
1	**10b**	Fe_3O_4@OA-Pd (0.38 mol%)	DMF/*t*-BuOK/120 °C	7	96	46
2		MNPs-Mel-Pd (20 mg)	DMF/K_2CO_3/100 °C	8	93	47
3		HMS-OPPh$_2$-Pd (0.5 mol%)	NMP[a]/K_2CO_3/120 °C	5	70	6
4		$Fe_3O_4@O_2PO_2(CH_2)_2NH_2$ (10 mg)	CH_3CN/K_2CO_3/Reflux	3	92	48
5		$Fe_3O_4@SiO_2$/Schiff base/Pd(II) (0.3 mol%)	DMF/K_2CO_3/110 °C	4	91	49
6		$Pd(OAc)_2$ (2 mol%)	H_2O/[ADPPy][OH][b]/80 °C	2	98	50
7		palladium(II)-exchanged zeolite-Y (EPdL1-Y) (0.7 mol%)	DMF/Na_2CO_3/140 °C	20	65	51
8		Pd/MOP-I (0.0174 mol%)	DMF/*n*-dodecane/Et_3N/110 °C	10	78	52
9		CuI (8.0 mol%)	DMSN/K_3PO_4/110 °C	24	70	53
10		**$NiFe_2O_4@SiO_2@ZrO_2/SO_4^{2-}/Cu/Co$ (0.005 mol% Cu, 0.01 mol% Co)**	**H_2O/K_3PO_4/60 °C**	**1**	**92**	**Present study**
11	**36c**	Fe_3O_4/P(GMA-AA-MMA)-Schiff base-Pd (0.1 mol%)	DMF/H_2O/K_2CO_3/80 °C	3	43	54
12		CL-Sc-Pd (0.005 mol%)	MW/K_2CO_3/50 °C	0.1	39	55
13		AC-Pd (0.06 mol%)	MW/K_2CO_3/400w	0.13	52	56
14		MNP@SPGMA@AP@Pd (0.1 mol%)	DMF/H_2O/K_2CO_3/70 °C	6	48	57
15		HCP-Pd-I (40 mg)	H_2O/K_3PO_4/80 °C	1	88	58
16		Pd@COF-QA (1.7 mol%)	H_2O/TEA[c]/50 °C	6	62	59[d]
17		**$NiFe_2O_4@SiO_2@ZrO_2/SO_4^{2-}/Cu/Co$ (0.005 mol% Cu, 0.01 mol% Co)**	**H_2O/K_3PO_4/60 °C**	**2.5**	**79**	**Present study**
18	**22a**	Silica-supported NHC-Pd/IL (1 mol%)	NMP[a]/NaOAc/Ar atmosphere/140 °C	9	95	60
19		Pd@NaY (1 mol%)	*n*-Butyl levulinate/Et_3N/150 °C	6	95	61
20		Si-OPPh$_2$-Pd (0.5 mol%)	NMP[a]/K_2CO_3/120 °C	1	88	6
21		$Fe_3O_4@SiO_2$-Se-T/Pd(II) (5 mg)	DMF/Et_3N/120 °C	0.75	95	62
22		Pd-MOT (1 mol%)	CH_3CN/K_2CO_3/80 °C	8	85	63
23		**$NiFe_2O_4@SiO_2@ZrO_2/SO_4^{2-}/Cu/Co$ (0.005 mol% Cu, 0.01 mol% Co)**	**H_2O/K_3PO_4/60 °C**	**0.7**	**92**	**Present study**
24	**50a**	$MnCl_2 \cdot 4H_2O$ (5 mol%) L-proline (10 mol%)	DMSO/NaOt-Bu/135 °C	24	72	64
25		**$NiFe_2O_4@SiO_2@ZrO_2/SO_4^{2-}/Cu/Co$ (0.005 mol% Cu, 0.01 mol% Co)**	**H_2O/K_3PO_4/60 °C**	**1.9**	**89**	**Present study**
26	**25b**	Pd–DABCO@SiO$_2$ (1 mol%)[e]	DMF/K_2CO_3/100 °C	6	91	65
27		Co@MicroCS (3 mol%)[f]	DMAc[g]/Et_3N/140 °C	8	82	66
28		MNPs-Mel-Pd (20 mg)	DMF/K_2CO_3/100 °C	8	88	67
29		Co-out-CNTs (20 mg)	PEG/K_2CO_3/60 °C	9	68	68
30		**$NiFe_2O_4@SiO_2@ZrO_2/SO_4^{2-}/Cu/Co$ (0.005 mol% Cu, 0.01 mol% Co)**	**H_2O/K_3PO_4/60 °C**	**3.2**	**87**	**Present study**

[a] *N*-Methyl-2-pyrrolidone. [b] 1-(4-Chlorophenyl)-3-methyl-4-phenyl-1,2,3-triazolium iodide. [c] Triethylamine. [d] R = OMe. [e] 1,4-Diazabicyclo[2.2.2]octane. [f] Aryl halide is iodobenzene. [g] Dimethylacetamide.

zirconium nanoparticles to magnetic nanoparticles, a significant increase in the efficiency was observed (Table 5, entry 13).

To confirm the advantage of the catalytic properties of $NiFe_2O_4@SiO_2@ZrO_2/SO_4^{2-}/Cu/Co$ for the Heck, Suzuki, and C–N coupling reactions, this was compared with the works of other researchers. The results are shown in Table 6.

Of the advantages of the $NiFe_2O_4@SiO_2@ZrO_2/SO_4^{2-}/Cu/Co$ catalyst over other previous reports, mentions could be made of the short time, high efficiency, green solvent, low metal toxicity, and easy catalyst recycling.

3.4. Mechanism study

The incorporation of Cu with various transition metals in heterobimetallic Cu complexes appears in the newest generation structures. The synergetic interactions between the active metal sites that have emerged as an effective approach in cross-couplings depend on the transition metal electropositivity or electronegativity of the latter rates of the distinct steps of the mono catalytic cycle (*e.g.*, reductive elimination or oxidative addition).[69] The interaction may be increased with the organic linker, which bridges to the different metal centers and plays a sensitive charge transfer role. The predicted result of this cooperation would be an enhancement of the overall reaction rate, so an increase in the activity of the heterobimetallic catalysts can be seen.[70]

This perspective contribution is timely, as the bimetallic catalysis for C–C and C–N coupling is a growing area that plays an important role in contributions to the synthetic implement.[71,72]

3.4.1. 1,2-Diphenylethene derivatives (10a-33c):. Based on the previous reports,[67,73] and also according to our results, we put forward a possible explanation for the Mizoroki–Heck cross-coupling reactions in Scheme 3a. The start of the reaction was assumed to be based upon an *in situ* reduction of Cu(II)

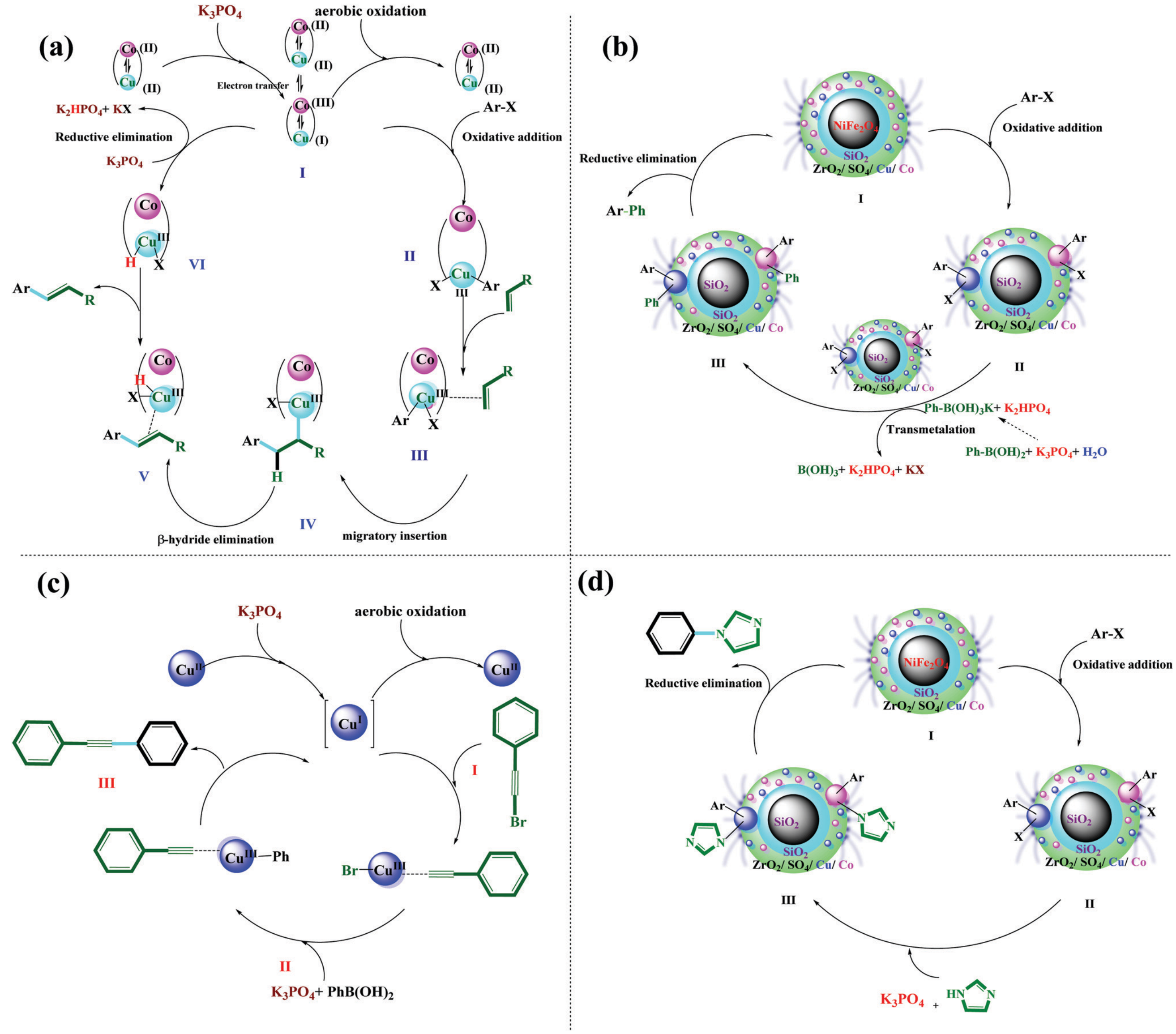

Scheme 3 A plausible mechanism for the (a) Mizoroki–Heck cross-coupling, (b) Suzuki coupling, (c) synthesis of internal alkynes, and (d) *N*-arylation of imidazole using $NiFe_2O_4@SiO_2@ZrO_2/SO_4^{2-}/Cu/Co$.

sites, which resulted in the Cu(I) species (I). This reduction was made by the copper(I) species responsible for the coupling reaction being begotten by an electron transfer from cobalt(II) and oxidation to cobalt(III), while in the opposite case, the formation of the copper(III) species at first seems unlikely. It was clear from the previous study that the active Cu(I) species would proceed with the cross-coupling reaction. In the following level, the low valent Cu(I) was oxidatively added into the aryl halide to cope with the aryl cobalt intermediate (II). In the next levels, olefin coordination with (II) and migratory insertion led to the shaping of adducts (III) and (IV), respectively. Hydridocobalt(VI) and a new olefin were compatible with, following β-hydride elimination. In the end, the active Cu(I) species (I) were regenerated by a reductive elimination in the presence of K_3PO_4. To complete the catalytic cycle for the Mizoroki–Heck cross-coupling reaction, aerobic oxidation of the Cu(I) species (I) to the Cu(II) complexes were conducted. Similar mechanisms for the synthesis of other compounds are shown in Scheme 3b–d.

3.5. Recoverability studies

Sustainability, durability, and recycling of a heterogeneous catalyst, as well as being energy-saving and environmentally friendly are prominent and important factors for the catalysts. The rigid mineral structure of sulfated zirconium oxide combined with the magnetic properties of $NiFe_2O_4$ make the catalyst recyclable and reusable, and minimizes any metal leaching. The catalyst recyclability was tested in the Heck reaction. The reaction of styrene and iodobenzene in the presence of K_3PO_4 base at 60 °C in each catalyst cycle was recovered. The recovered catalyst was washed with EtOH (2 × 5 mL) and was reused in the next step without any purification or pre-activation. Fig. 11 shows the corresponding results for more than ten consecutive periods without significant loss of efficiency (catalyst performance and reaction performance). Finally, after 11 consecutive periods, the product yield reached 87% (6% decrease) (Heck coupling). Also, FE-SEM, TEM, and FTIR analyses were taken from the recycled catalyst after 11 consecutive runs. The results have shown the stability of the $NiFe_2O_4$@SiO_2@$ZrO_2/SO_4{}^{2-}$/Cu/Co catalyst in organic and aqueous environments. These results have indicated a rigid and durable structure for the $NiFe_2O_4$@SiO_2@$ZrO_2/SO_4{}^{2-}$/Cu/Co catalyst as a magnetic heterogeneous nanocatalyst. Another benefit of the cobalt copper catalyst is its high recycling frequency and low leaching. The results were compared with other catalysts mentioned in the existing literature (Table 7).

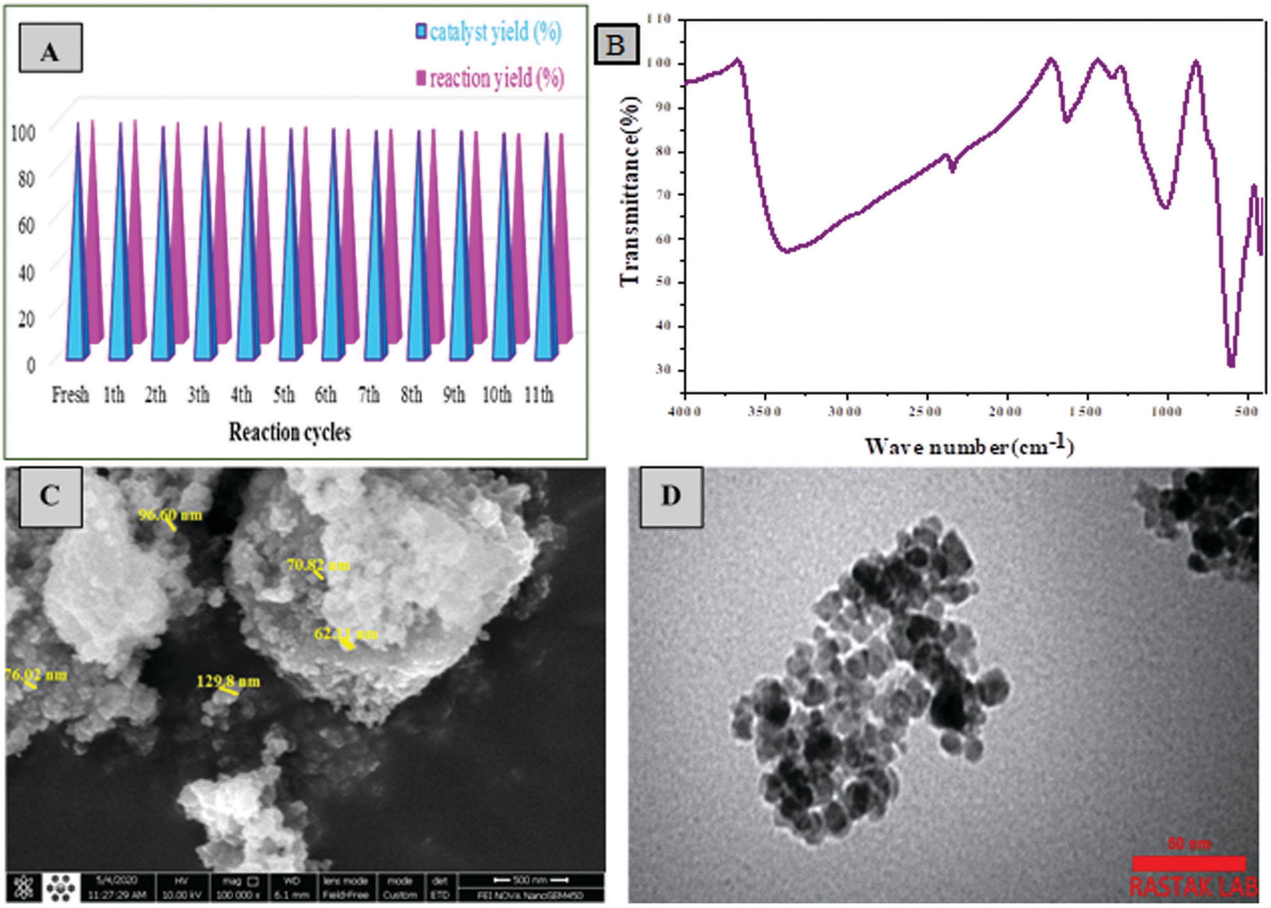

Fig. 11 (A) Recovery and reusability of $NiFe_2O_4$@SiO_2@$ZrO_2/SO_4{}^{2-}$/Cu/Co in the Mizoroki–Heck cross-coupling reaction under optimized reaction conditions. (B) FTIR spectrum, (C) FE-SEM, and (D) TEM images of the recovered catalyst after the 11th run.

Table 7 Reproducibility of the different Cu and Co catalysts in the Heck reactions

Entry	Catalyst	Recycle	Yield (%)	Ref.
1	Fe_3O_4@SiO_2@PrNCu	6	91–83	17
2	MNP@PAMAM-Co	5	90–85	12
3	Co-MS@MNPs/CS	5	88–83	67
4	Cu-NH_2-GO	6	88–66	18
5	Schiff Base/CuI	5	93–86	74
6	Co-DMM@MNPs/Cs	6	82–62	2
7	Fe_3O_4@SiO_2@Im[Cl]Co(III)-melamine nanocomposite	7	91–89	75
8	Magnetic Chitosan Cobalt	6	92–87	67
9	Fe_3O_4@SiO_2-Isa Cu(II)	5	98–92	76
10	**$NiFe_2O_4$@SiO_2@ZrO_2/SO_4^{2-}/Cu/Co**	**11**	**93–87**	**This work**

4. Conclusion

In the end, we synthesized a magnetically recyclable bimetallic nanocatalyst consisting of various Lewis acid and Brønsted acid active sites. The catalyst can be used as a special catalyst in the Heck-Suzuki reaction and the coupling of C–N cross-couplings. The reactions can be performed from various precursors by a green solvent, short reaction times, and with high efficiency (49–94%), without the formation of any by-products. These results were viewed as irrespective of the presence of electron-donating and electron-withdrawing groups in the evaluated (pre)catalyst structures. The transfer of an electron between the Cu, Co, and Zr metal sites can be responsible for the oxidation addition and reductive elimination proposed mechanism, which is in line with the reported mechanisms. Moreover, *via* adsorption of the cation, a surface-mediated/facilitated interconversion was made among the sulfate ions on the catalyst with the function of the base in water. The running methodology can be replaced with the expensive Pd catalytic systems with highly toxic and expensive phosphine ligands to catalyze the Heck, Suzuki, and C–N cross-coupling reactions. K_3PO_4 as a cheaper and safer base source than Et_3N, and others was used. The reactions were carried out in water at 60 °C in the presence of 0.003 g (0.005 mol% Cu, 0.01 mol% Co) of $NiFe_2O_4$@SiO_2@ZrO_2/SO_4^{2-}/Cu/Co magnetic nanocatalyst. The activity of the catalyst was evaluated by various control experiments, and the magnetic nanocatalyst was characterized by XRD, FE-SEM, EDX mapping, BET, TEM, HRTEM, FTIR, TGA, and VSM. The catalyst was recycled more than ten times, and there was no change in the catalyst features and essence. The recycled catalyst was characterized with FE-SEM, TEM, and FTIR analysis. This should be noted that the catalytic activity in other organic transformations is being investigated in an ongoing research project.

Conflicts of interest

There are no conflicts to declare.

Acknowledgements

The authors are grateful to the University of Birjand for financial support.

References

1 E. Ocansey, J. Darkwa and B. C. E. Makhubela, *Polyhedron*, 2019, **166**, 52–59.
2 Q. Yang, N. Sane, D. Klosowski, M. Lee, T. Rosenthal, N. X. Wang and E. Wiensch, *Org. Process Res. Dev.*, 2019, **23**, 2148–2156.
3 M. A. Nasseri, S. A. Alavi, M. Kazemnejadi and A. Allahresani, *RSC Adv.*, 2019, **9**, 20749–20759.
4 K. Köhler, M. Wagner and L. Djakovitch, *Catal. Today*, 2001, **66**, 105–114.
5 J. K. Vandavasi, X. Hua, H. Ben Halima and S. G. Newman, *Angew. Chem., Int. Ed.*, 2017, **56**, 15441–15445.
6 F. Farjadian, M. Hosseini, S. Ghasemi and B. Tamami, *RSC Adv.*, 2015, **5**, 79976–79987.
7 E. J. Farrington, J. M. Brown, C. F. J. Barnard and E. Rowsell, *Angew. Chem.*, 2002, **114**, 177–179.
8 M. Nasrollahzadeh, S. M. Sajadi, A. Rostami-Vartooni and M. Khalaj, *RSC Adv.*, 2014, **4**, 43477–43484.
9 S. H. Tsai, Y. H. Liu, P. L. Wu and C. S. Yeh, *J. Mater. Chem.*, 2003, **13**, 978–980.
10 L. Feng, H. Chong, P. Li, J. Xiang, F. Fu, S. Yang, H. Yu, H. Sheng and M. Zhu, *J. Phys. Chem. C*, 2015, **119**, 11511–11515.
11 M. A. Nasseri, M. Kazemnejadi, B. Mahmoudi, F. Assadzadeh, S. A. Alavi and A. Allahresani, *J. Nanopart. Res.*, 2019, **21**, 1–14.
12 M. Arghan, N. Koukabi and E. Kolvari, *Appl. Organomet. Chem.*, 2019, **33**, e4823.
13 M. Corpet and C. Gosmini, *Chem. Commun.*, 2012, **48**, 11561–11563.
14 N. Rajesh, N. Barsu and B. Sundararaju, *Tetrahedron Lett.*, 2018, **59**, 862–868.
15 K. Lévay and L. Hegedűs, *Curr. Org. Chem.*, 2019, **23**, 1881–1900.
16 A. Baccalini, S. Vergura, P. Dolui, G. Zanoni and D. Maiti, *Org. Biomol. Chem.*, 2019, **17**, 10119–10141.
17 I. Yavari, A. Mobaraki, Z. Hosseinzadeh and N. Sakhaee, *J. Organomet. Chem.*, 2019, **897**, 236–246.
18 R. M. Ansari and B. R. Bhat, *Chem. Phys.*, 2019, **517**, 155–160.
19 V. Sadhasivam, B. Sankar, G. Elamathi, M. Mariyappan and A. Siva, *Res. Chem. Intermed.*, 2020, **46**, 681–700.
20 J. C. Park, A. Kim, S. Jang, J.-I. Yang, S. W. Kang, C.-W. Lee, B.-H. Kim and K. H. Park, *ChemCatChem*, 2019, **11**, 991–996.
21 L. Liu, X. Zhou, L. Liu, S. Jiang, Y. Li, L. Guo, S. Yan and X. Tai, *Catalysts*, 2019, **9**, 538.
22 A. Berrichi, R. Bachir, S. Bedrane, N. Choukchou-Braham and K. Belkacemi, *Res. Chem. Intermed.*, 2019, **45**, 3481–3495.

23 W. Fu, Y. Cao, Q. Feng, W. R. Smith, P. Dong, M. Ye and J. Shen, *Nanoscale*, 2019, **11**, 1379–1385.
24 N. Gogoi, U. Bora, G. Borah and P. K. Gogoi, *Appl. Organomet. Chem.*, 2017, **31**, e3686.
25 H. Mahmoudi, F. Valentini, F. Ferlin, L. A. Bivona, I. Anastasiou, L. Fusaro, C. Aprile, A. Marrocchi and L. Vaccaro, *Green Chem.*, 2019, **21**, 355–360.
26 A. Galadima, R. P. K. Wells and J. A. Anderson, *Appl. Petrochem. Res.*, 2012, **1**(1–4), 35–43.
27 X. Li, K. Nagaoka, L. J. Simon, R. Olindo, J. A. Lercher, A. Hofmann and J. Sauer, *J. Am. Chem. Soc.*, 2005, **127**, 16159–16166.
28 Z. Ma, X. Meng, N. Liu, C. Yang and L. Shi, *Ind. Eng. Chem. Res.*, 2018, **57**, 14377–14385.
29 H. Ghafuri, A. Rashidizadeh and H. R. Esmaili Zand, *RSC Adv.*, 2016, **6**, 16046–16054.
30 C. Khatri, M. K. Mishra and A. Rani, *Fuel Process. Technol.*, 2010, **91**, 1288–1295.
31 Y. Wang, W. Zhang, C. Luo, X. Wu, Q. Wang, W. Chen and J. Li, *Ceram. Int.*, 2016, **42**, 17374–17381.
32 M. A. Nasseri, S. A. Alavi, M. Kazemnejadi and A. Allahresani, *ChemistrySelect*, 2019, **4**, 8493–8499.
33 M. K. Mishra, B. Tyagi and R. V. Jasra, *Journal of Molecular Catalysis A: Chemical*, Elsevier, 2004, vol. 223, pp. 61–65.
34 F. Heshmatpour and R. B. Aghakhanpour, *Adv. Powder Technol.*, 2012, **23**, 80–87.
35 M. A. Nasseri, M. Kazemnejadi, B. Mahmoudi, F. Assadzadeh, S. A. Alavi and A. Allahresani, *J. Nanopart. Res.*, 2019, **21**, 1–14.
36 N. Hosseini Nasab and J. Safari, *J. Mol. Struct.*, 2019, **1193**, 118–124.
37 R. F. Perez, S. J. Canhaci, L. E. P. Borges and M. A. Fraga, *Catal. Today*, 2017, **289**, 273–279.
38 G. Shi, F. Yu, Y. Wang, D. Pan, H. Wang and R. Li, *Renewable Energy*, 2016, **92**, 22–29.
39 L. Zare Fekri and A. R. Darya-Laal, *Polycyclic Aromat. Compd.*, 2020, **40**, 1539–1556.
40 Y. Xiao, J. Zai, B. Tian and X. Qian, *Springer*, 2017, **9**, 34.
41 H. Y. Zhu, R. Jiang, Y. Q. Fu, R. R. Li, J. Yao and S. T. Jiang, *Appl. Surf. Sci.*, 2016, **369**, 1–10.
42 S. Iraqui, S. S. Kashyap and M. H. Rashid, *Nanoscale Adv.*, 2020, **2**, 5790–5802.
43 S. Li, J. Pan, F. Li, L. Zhang, D. Chai, Z. Zhang and J. Xin, *Dalton Trans.*, 2020, **49**, 10203–10211.
44 X. Xu, Y. Li, G. Zhang, F. Yang and P. He, *Water*, 2019, **11**, 384.
45 D. R. Lima, N. Jiang, X. Liu, J. Wang, V. A. S. Vulcani, A. Martins, D. S. Machado, R. Landers, P. H. C. Camargo and A. Pancotti, *ACS Appl. Mater. Interfaces*, 2017, **9**, 39830–39838.
46 E. Rafiee and M. Kahrizi, *J. Mol. Liq.*, 2016, **218**, 625–631.
47 M. A. Bodaghifard, *J. Organomet. Chem.*, 2019, **886**, 57–64.
48 M. Aghayee, M. A. Zolfigol, H. Keypour, M. Yarie and L. Mohammadi, *Appl. Organomet. Chem.*, 2016, **30**, 612–618.
49 M. Esmaeilpour and J. Javidi, *J. Chin. Chem. Soc.*, 2015, **62**, 614–626.
50 D. S. Gaikwad, K. A. Undale, D. B. Patil and D. M. Pore, *J. Iran. Chem. Soc.*, 2019, **16**, 253–261.
51 S. Kumari, K. Maddipoti, B. Das and S. Ray, *Inorg. Chem.*, 2019, **58**, 1527–1540.
52 S. Ding, B. Qu, Y. Li, L. Sun, S. Wu, R. Zeng, M. Xu, C. Chen and N. Zhang, *New J. Chem.*, 2019, **43**, 14674–14677.
53 S. Cheng, W. Wei, X. Zhang, H. Yu, M. Huang and M. Kazemnejadi, *Green Chem.*, 2020, **22**, 2069–2076.
54 D. Yuan, L. Chen, L. Yuan, S. Liao, M. Yang and Q. Zhang, *Chem. Eng. J.*, 2016, **287**, 241–251.
55 N. Yılmaz Baran, T. Baran and A. Menteş, *Appl. Catal., A*, 2017, **531**, 36–44.
56 T. Baran, *Int. J. Biol. Macromol.*, 2019, **127**, 232–239.
57 A. Pourjavadi, A. Motamedi, Z. Marvdashti and S. H. Hosseini, *Catal. Commun.*, 2017, **97**, 27–31.
58 X. Liu, W. Xu, D. Xiang, Z. Zhang, D. Chen, Y. Hu, Y. Li, Y. Ouyang and H. Lin, *New J. Chem.*, 2019, **43**, 12206–12210.
59 J. C. Wang, C. X. Liu, X. Kan, X. W. Wu, J. L. Kan and Y. Bin Dong, *Green Chem.*, 2020, **22**, 1150–1155.
60 B. Karimi and D. Enders, *Org. Lett.*, 2006, **8**, 1237–1240.
61 R. Marcel, T. Durillon, L. Djakovitch, F. Fache and F. Rataboul, *ChemistrySelect*, 2019, **4**, 3329–3333.
62 Y. Rangraz, F. Nemati and A. Elhampour, *New J. Chem.*, 2018, **42**, 15361–15371.
63 O. A. Alimi, C. A. Akinnawo and R. Meijboom, *New J. Chem.*, 2020, **44**, 18867–18878.
64 F. F. Yong and Y. C. Teo, *Tetrahedron Lett.*, 2010, **51**, 3910–3912.
65 S. Jadhav, S. Patil, A. Kumbhar, S. Kamble and R. Salunkhe, *Transition Met. Chem.*, 2019, **44**, 507–514.
66 Y. Bao, L. Shao, G. Xing and C. Qi, *Int. J. Biol. Macromol.*, 2019, **130**, 203–212.
67 A. R. Hajipour, F. Rezaei and Z. Khorsandi, *Green Chem.*, 2017, **19**, 1353–1361.
68 A. R. Hajipour, Z. Khorsandi and H. Farrokhpour, *New J. Chem.*, 2019, **43**, 8215–8219.
69 R. K. Rai, D. Tyagi, K. Gupta and S. K. Singh, *Catal. Sci. Technol.*, 2016, **6**, 3341–3361.
70 D. R. Pye and N. P. Mankad, *Chem. Sci.*, 2017, **8**, 1705–1718.
71 L. X. You, H. J. Liu, L. X. Cui, F. Ding, G. Xiong, S. J. Wang, B. Y. Ren, I. Dragutan, V. Dragutan and Y. G. Sun, *Dalton Trans.*, 2016, **45**, 18455–18458.
72 N. P. Mankad, *Chem. Commun.*, 2018, **54**, 1291–1302.
73 A. K. Srivastava, N. Satrawala, M. Ali, C. Sharma and R. K. Joshi, *Tetrahedron Lett.*, 2019, **60**, 151283.
74 Y. Wang and M. Zhang, *ChemistrySelect*, 2019, **4**, 9673–9676.
75 M. Kazemnejadi, S. A. G. Alavi, Z. Rezazadeh, M. A. Nasseri, A. Allahresani and M. Esmaeilpour, *Green Chem.*, 2019, **21**, 1718–1734.
76 S. Simin MIRI, M. Khoobi, F. Ashouri, F. Jafarpour, P. Rashidi Ranjbar and A. Shafiee, *Turk. J. Chem.*, 2015, **39**, 1232–1246.